A Review of Recent Developments in Neuromorphic Computing Based on Emerging Memory Devices

Jingru Sun[1,2*], Jingwen Sun[1,2], Xiaosong Li[1,2], Yichuang Sun[3], Qinghui Hong[1], Chunhua Wang[1]

[1*]College of Computer Science and Electronic Engineering, Hunan University, Changsha, 410082, China.
[2]Chongqing Research Institute, Hunan University, Chongqing, 401120, China.
[3]School of Engineering and Computer Science, University of Hertfordshire, Hatfield, AL10 9AB, UK.

*Corresponding author(s). E-mail(s): jt_sunjr@hnu.edu.cn;
Contributing authors: jingwen513@hnu.edu.cn; liguangbi@hnu.edu.cn; y.sun@herts.ac.uk; hongqinghui@hnu.edu.cn; wch1227164@hnu.edu.cn;

Abstract

Neuromorphic computing is a novel computing paradigm that mimics biological neural systems' structure and information processing mechanisms. By leveraging highly parallel, low-power, brain-inspired architectures, neuromorphic computing provides efficient hardware support for artificial intelligence (AI). Within this framework, the synapse and neuron models and their circuit implementations are the foundational core of neuromorphic computing, significantly influencing its performance and capabilities. This paper reviews recent advances in neuron model circuits and the development of neuromorphic computing. Specifically, we discuss: 1) the basic working principles and implementation methods of synapses; 2) the biomimetic characteristics and physical circuits of various neuron models; 3) neural networks and corresponding dynamics analysis. Finally, future research directions for neuron model design and neuromorphic networks are discussed.

Keywords: Neuromorphic computing, synapse, neuron model, neural network, memristor

1 Introduction

With the exponential growth in AI-driven computational demands, the memory wall problem in traditional von Neumann architectures has become increasingly prominent [1]. Meanwhile, as complementary metal oxide semiconductor (CMOS) technology approaches its physical limits, the failure of Dennard scaling will lead to stagnation in improvements in energy efficiency [2]. To overcome these limitations, neuromorphic computing —a new computational paradigm inspired by the biological brain —has emerged as a promising solution [3].

The biological brain possesses many fascinating advantages, including high computational capacity, self-adaptation, parallel processing, ultralow power consumption, nonlinearity, and high robustness [4], as illustrated in Fig. 1. The human brain contains 86 billion neurons, each with more than 10,000 synapses [5, 6]. Neurons are the fundamental units of the brain and are connected

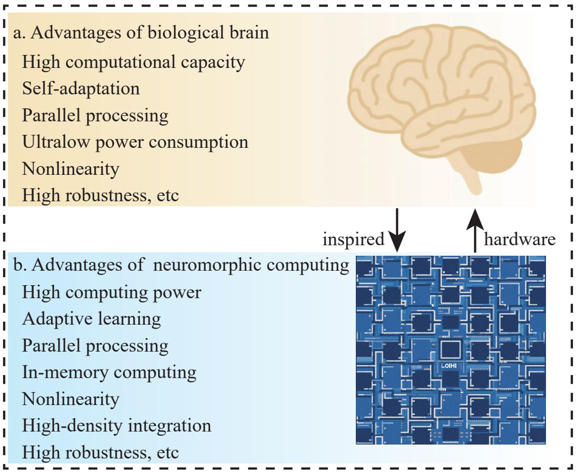

Fig. 1 Biological brain vs. Neuromorphic computing.

through synapses, collectively forming the core foundational units of the brain's computational processes. Advanced functions, such as cognition, memory, and decision-making, are primarily achieved through the dynamics of neuron-synapse networks [7–10]. The bio-inspired architecture of neuromorphic computing attempts to construct computing units and connections similar to the biological brain, and correspondingly has advantages such as high computing power, adaptive learning, parallel processing, in-memory computing, nonlinearity, high-density integration, and high robustness, etc. Neuromorphic computing can be considered from the following three aspects: device design of synapse; modeling of neurons and corresponding circuit node implementations; neural network constructions and their dynamics analysis.

Traditional neuromorphic computing relies entirely on CMOS technology, resulting in energy efficiency far lower than that of the biological brain [11, 12]. In recent years, memory devices such as memristors and novel transistors have emerged as promising research directions in neuromorphic computing due to their non-volatility, low power consumption, and nonlinearity.

This paper provides a detailed overview of the above three aspects and their development directions. The rest of the paper is organized as follows. Section II introduces memory devices for implementing synapses. Section III discusses neuron models and circuit implementation. Section IV

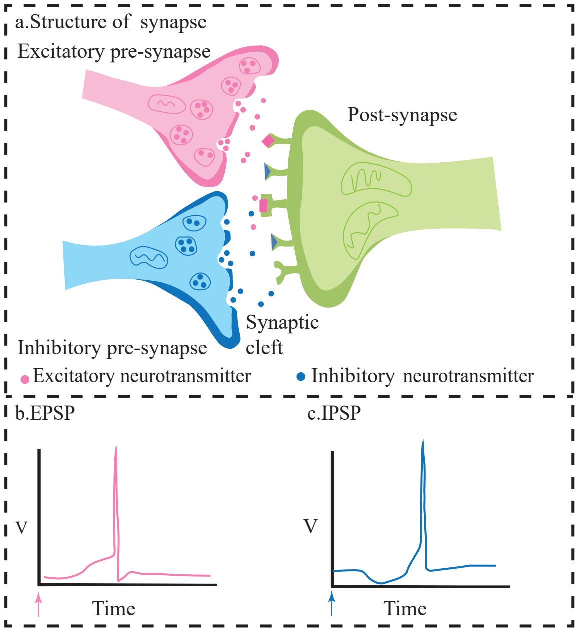

Fig. 2 Structure of synapse and EPSP/ IPSP.

explores neural network design and dynamics analysis. Section V provides a summary and outlook of the paper.

2 Implementation of Synapses

2.1 The Characteristics of Synapses

As shown in Fig. 2, synapse is a specialized junction facilitating communication between two neurons or a neuron and an effector cell. Structurally, it comprises three distinct components: the presynaptic membrane, the synaptic cleft, and the postsynaptic membrane [13]. The electrical signal from the presynaptic neuron is transmitted through the axon to the presynaptic membrane, triggering the release of neurotransmitters (e.g., glutamate, γ-Aminobutyric acid (GABA)) [14, 15] into the synaptic cleft. Neurotransmitters bind to the postsynaptic membrane, altering its permeability and causing changes in the postsynaptic current/potential. The release of excitatory neurotransmitters generates excitatory postsynaptic currents/potentials (EPSCs/ EPSPs), while the release of inhibitory neurotransmitters leads to inhibitory postsynaptic currents/potentials (IPSCs/ IPSPs). The sum of EPSCs and

IPSCs in the postsynaptic neuron determines whether it will generate an action potential (AP).

Synaptic plasticity is an activity-dependent change in the strength of neuronal connections, which has long been recognized as a crucial component of learning and memory [16–18]. Depending on the time scale of changes, plasticity can be divided into short-term plasticity (STP), which lasts for seconds to minutes, including paired pulse facilitation (PPF) and paired-pulse depression (PPD) [19], and long-term plasticity, which represents long-term changes in synaptic weight, including long-term potentiation (LTP) and long-term depression (LTD) [20]. The basic mechanisms of synaptic plasticity include Hebbian plasticity [21], spike-timing-dependent plasticity (STDP) [22] and its extensions, such as triplet-based STDP (T-STDP) [23, 24] and quadruplet-based STDP (Q-STDP) [25]. STDP involves a pair of presynaptic and postsynaptic spikes. If a spike from the presynaptic neuron precedes a spike from the postsynaptic neuron, the synaptic strength is potentiated, inducing LTP; conversely, it is depressed, inducing LTD. The smaller the interval between the spikes, the stronger the effect of synaptic modification. Synaptic weight changes can be expressed as follows and its timing diagram is shown in Fig. 3,

$$\Delta w = \begin{cases} A^{+}e^{-\frac{\Delta t}{\tau_{+}}}, & \text{if } \Delta t \geq 0 \\ -A^{-}e^{\frac{\Delta t}{\tau_{-}}}, & \text{if } \Delta t < 0 \end{cases} \tag{1}$$

where $\Delta t = t_{post} - t_{pre}$ represents the time difference between postsynaptic and presynaptic spikes. A^{+} and A^{-} represent the amplitude of the weight changes for potentiation and depression. τ_{+} and τ_{-} are the time constants.

T-STDP adds a third spike either in the presynaptic or postsynaptic neuron, which can describe plasticity that cannot be explained by the basic STDP. Synaptic weight changes can be expressed as follows and its timing diagram is shown in Fig. 3,

$$\Delta w = \begin{cases} e^{-\frac{\Delta t_1}{\tau_{+}}}(A_2^{+} + A_3^{+}e^{-\frac{\Delta t_2}{\tau_y}}), \\ \text{if } t = t_{post} \\ -e^{\frac{\Delta t_1}{\tau_{-}}}(A_2^{-} + A_3^{-}e^{-\frac{\Delta t_3}{\tau_x}}), \\ \text{if } t = t_{pre} \end{cases} \tag{2}$$

where $\Delta t_1 = t_{post}(n) - t_{pre}(n)$, $\Delta t_2 = t_{post}(n) - t_{post}(n-1)$, $\Delta t_3 = t_{pre}(n) - t_{pre}(n-1)$, A_2^{+} and

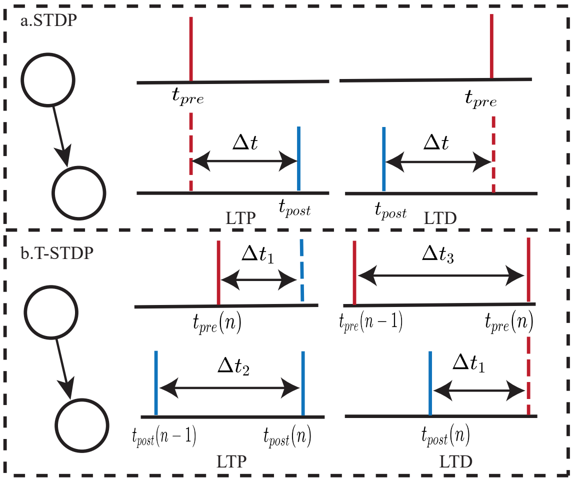

Fig. 3 Timing diagram of STDP and T-STDP.

A_2^{-} represent the amplitude of the weight changes whenever there is a pre-post pair or a post-pre pair. A_3^{+} and A_3^{+} represent the amplitude of the triplet term for potentiation and depression, respectively. τ_{+}, τ_{-}, τ_y and τ_x are corresponding time constants.

Other plasticity mechanisms include spike-rate-dependent plasticity (SRDP), spike-number-dependent plasticity (SNDP), spike-voltage-dependent plasticity (SVDP), three-factor plasticity rule, supervised synaptic plasticity, behavioral timescale synaptic plasticity (BTSP) [26], and homeostatic plasticity [27]. The strength of synaptic connections determines the efficiency of signal transmission in neural networks.

2.2 Memristive Synapses

Synapses based on CMOS technology face several limitations, including a large area, high power consumption, and poor biological plausibility. In contrast, memristors possess advantages such as nonvolatility, compact size, nonlinearity, variable resistance, and low power consumption, etc [28, 29]. Synaptic implementations based on memristors can be divided into two complementary categories: one utilizes physical devices to achieve synaptic functions, and the other simulates synaptic connections between neurons using mathematical models and performs dynamics analysis.

In 1971, Professor Chua first proposed the concept of memristor [30, 31], which was experimentally validated by HP in 2008 [32]. Subsequently, researchers have proposed various memristor models, such as Chua's memristor [33], spin memristors [34, 35], threshold switching models [36, 37], tunneling barrier models [38], and locally active memristors (LAMs) [39].

In terms of physical devices, memristors can be broadly categorized into oxide-based, halide perovskite-based, chalcogenide-based, and organic-based, etc. These memristors exhibit different characteristics in synaptic simulation based on their materials. A comparison of various types of memristors is presented in Table. 1. In terms of dynamics analysis, local activity is considered the origin of complexity [40]. In addition, K^+ and Na^+ channels on axons have been proved to be LAMs [41, 42]. Therefore, it is of great significance to simulate synapses and conduct dynamics analysis using LAMs.

2.2.1 Oxide-Based Memristors

Oxide-based memristors use oxides as the dielectric layer and are the most common type of memristor. These oxides include SiO_x, TiO_x, ZnO_x, HfO_x, TaO_x, ZrO_x, CeO_x and others. The resistive switching mechanism of oxide-based memristors depends on the formation and rupture of conductive filaments (CFs) during operation, where the CF can be composed of metal or oxygen vacancies.

In 2016, Wang et al. developed a diffusive Ag-in-oxide memristor, which can emulate synaptic Ca^{2+} dynamics. A single memristor can directly simulate STP, and when connected in series with a drift-type memristor, it can simulate long-term plasticity, SRDP, and STDP [43]. This device simulates synaptic behaviors more realistically than previous devices, but it realizes less synaptic functions. In 2018, Yin et al. studied a bilayer memristor based on $W/HfO_y/HfO_x/Pt$, whose structure and oxygen vacancy distribution mimic the complete synapse and Ca^{2+} distribution, respectively. This device can achieve more synaptic functions, including SRDP, STDP, PPF, PPD, LTP, and LTD [44]. Beyond merely simulating synapses, oxide-based memristors can also be used to simulate nociceptors, which expands the applications of memristors. In 2023, Sahu et al. demonstrated a TiO_2 memristor that can exhibit volatile switching, non-volatile switching, and controllable conversion between them. The delay dynamics during volatile switching are utilized to simulate nociceptive functions. This memristor can also achieve synaptic short-term memory (STM), long-term memory (LTM), SRDP, and STDP [45].

Oxide-based memristors have many compelling advantages. First, the high similarity between their physical mechanisms and the ion movement in biological synapses enables them to realistically simulate the complex functions of synapses. Second, low latency promotes real-time applications. Then, due to the abundance of materials and a relatively simple manufacturing process, they have a lower cost. Finally, they possess significant integration potential due to their high scalability and compatibility with CMOS technology.

2.2.2 Halide Perovskite-Based Memristors

Halide Perovskite materials possess a typical ABX_3-type crystal structure, in which the lattice is composed of octahedra connected by shared vertices. They exhibit unique optoelectronic properties, such as high light absorption coefficient, direct band gap, long carrier diffusion lengths, low defect density, and a soft lattice structure that enables high mobility of ions within the material. Halide perovskites mainly include $CsPbBr_3$, $MAPbI_3$, $Cs_2AgBiBr_6$, and $CsSnI_3$. Their resistive switching mechanisms not only involve CF similar to that in oxide-based memristors, but also include the trapping and de-trapping of charges, ion or vacancy migration.

In 2016, Xiao et al. reported an organometal trihalide perovskite synaptic device based on indium tin oxide (ITO)/poly(3,4-ethylenedioxythiophene)-poly(styrenesulfonate) (PEDOT:PSS)/$MAPbI_3$/Au structure. This device can achieve STDP, STP, LTP, and light-readout SRDP [46]. This method provides an optical readout in addition to electrical pulses, but it has not yet utilized light to modulate synaptic functions. In 2020, Gong et al. fabricated a memristor composed of $CsPbBr_3$, Al_2O_3, and pentacene. This memristor can achieve LTP, LTD, STDP and light-enhanced PPF [47]. Additionally, it enables precise control over synaptic functions based on perovskite quantum dots (QDs). 3D perovskites have poor environmental stability due to its sensitivity to moisture, light, and temperature. Therefore, 2D perovskites have been proposed. In 2022, Kim et al. demonstrated vertically aligned 2D halide perovskite films using phenethyl-ammonium (PEA) and fabricated an ITO/$PEA_2MA_{n-1}Pb_nI_{3n+1}$/Au memristor. This device can achieve spike width-dependent plasticity (SWDP), SVDP, STP, and long-term plasticity, and STDP [48].

Halide perovskite-based memristors with photoelectric-coupled plasticity can be utilized to realize neuromorphic vision systems. Furthermore, 2D perovskites exhibit excellent environmental stability. Finally, perovskite materials can be synthesized on nearly any substrate, making them suitable for integration with CMOS.

2.2.3 Chalcogenide-Based Memristors

Chalcogenide-based memristors are diverse, with typical representatives including GeSbTe (GST), a kind of chalcogenide glass, and MoS_2, $MoTe_2$, WS_2, which are transition metal dichalcogenides. Their resistive switching mechanisms mainly cover three types: formation and rupture of CF, the reversible phase transition between crystalline and amorphous states, and trapping, de-trapping of charges.

GST is a widely used phase-change material, and different conductance levels can be achieved by controlling the degree of crystallization. In 2012, Kuzum et al. fabricated a W/GST/TiN memristor that can achieve precise control of resistance with 100 resistance levels, and synaptic STDP and LTP [49]. Transition metal dichalcogenides are novel 2D material, which has a thinner thickness, faster switching speed, and richer synaptic functions compared to GST. In 2019, Yan et al. fabricated a Pd/WS_2/Pt device, and it successfully mimics PPF, STDP, and STP-LTP [50]. In 2023, Yu et al. fabricated a memristor based on Ag/$MoTe_2$/ITO structure. This device has a multi-resistance level and can achieve LTP, LTD, STDP, STP, post-tetanic potentiation (PTP) [51].

Chalcogenide-based memristors exhibit continuously tunable resistances, allowing for precise mimicry of synaptic weight gradation, which is beneficial for constructing high-precision neural networks. Furthermore, their ultrafast switching capability enables rapid responses of synapses on a nanosecond scale. Finally, they can respond to multimodal signals.

2.2.4 Organic-Based Memristors

The materials used for organic-based memristors mainly include polymers, such as PEDOT:PSS, polyaniline (PANI), polyvinyl alcohol (PVA), organic small molecules, such as 2-amino-4,5-imidazoledicarbonitrile (AIDCN), bis-4-(N-carbazolyl)phenyl)phenylphosphine oxide (BCPO), Benzene-1,3,5-tricarboxylic acid (TMA), and proteins such as silk fibroin, albumin, ferritin. Their switching mechanisms include formation and rupture of CF, charges trapping/de-trapping, charge transfer, conformational reconfiguration, and redox reaction.

In 2016, Zhang et al. fabricated Ta/ethyl viologen diperchlorate [$EV(ClO_4)_2$]/triphenylamine-based polyimide (TPA-PI)/Pt memristor, and it is capable of bearing 100 bending cycles. This device can achieve STP, LTP, and LTD [52]. Organic small molecules feature design flexibility and solution processability. In 2019, Mao et al. fabricated a ITO/BCPO/Al/Au memristor, in which BCPO is compatible with flexible substrates. This device can achieve SRDP, PPF, LTP, and STDP [53]. Compared to polymers, protein materials exhibit more pronounced biocompatibility and biodegradability. Yan et al. fabricated a transparent and flexible W/egg albumen/ITO/polyethylene terephthalate (PET) memristor, which can be bent 1000 times. This memristor can achieve EPSC, PPF, PPD, LTP [54].

Organic-based memristors exhibit excellent flexibility, and other advantages such as low cost, light weight, solution-processability, demonstrating unique application potential in fields like flexible electronics, wearable devices, and biomedical implantable devices.

2.2.5 Locally Active Memristors

LAMs are defined to be any memristor that exhibits a negative memductance or a negative memristance for at least some value of the memristor voltage, or memristor current. Some devices based on VO_2 and NbO_2 have been proven to be LAMs [55, 56]. LAMs have many mathematical models, such as the Chua-Corsage Memristor shown below, and they are used for synaptic connections and dynamics analysis.

The state-dependent Ohm's law and state equation of the Chua-Corsage Memristor are as follows. The DC V–I curve is shown in Fig. 4. It

Table 1 Comparison of different types of memristors.

Type	Structure	Mechanism	Function	Energy	Ref
Oxide	$Pt/SiO_xN_y/Ag/Pt$	CF	STP	–	[43]
	$W/HfO_y/HfO_x/Pt$	CF	SRDP, STDP, PPF, PPD, LTP, LTD	5fJ	[44]
	$Ag/TiO_2/Pt/Ti/SiO_2/Si$	CF	STM, LTM, SRDP, STDP	3.76pJ	[45]
Halide perovskite	ITO/PEDOT:PSS/ $MAPbI_3/Au$	CF	STDP, STP, LTP, SRDP	∼fJ	[46]
	Au/Pentacene/ $Al_2O_3/CsPbBr_3/SiO_2$	Hole trapping/de-trapping	LTP, LTD, PPF, STDP	–	[47]
	$ITO/PEA_2MA_{n-1}Pb_nI_{3n+1}/Au$	Vacancy migration	SWDP, SVDP, STP, STDP	–	[48]
Chalcogenide	W/GST/TiN	Phase transition	STDP, LTP	1pJ	[49]
	$Pd/WS_2/Pt$	CF	PPF, STDP, STP-LTP	∼fJ	[50]
	$Ag/MoTe_2/ITO$	CF	LTP, LTD, STDP, STP, PTP	74.2pJ	[51]
Organics	$Ta/EV(ClO_4)_2$/TPA-PI/Pt	redox reaction	STP, LTP, LTD	–	[52]
	ITO/BCPO/Al/Au	CF	SRDP, PPF, LTP, STDP	–	[53]
	W/egg albumen/ITO/PET	CF	PPF, PPD, LTP	20nJ	[54]

contains a negative slope over the range of $-10\,\mathrm{V} < V < -3.334\,\mathrm{V}$ and when $-7.09\,\mathrm{V} < V < -6.9\,\mathrm{V}$, the slope is approximately -33mS [57].

State-Dependent Ohm's Law:

$$i = G(x)v \tag{3}$$

where

$$G(x) = G_0 x^2 \tag{4}$$

State Equation:

$$\frac{dx}{dt} = 30 - x + |x - 20| - |x - 40| + v \triangleq h(x, v) \tag{5}$$

where x is the state variable, $G(x)$ and $h(x, v)$ are functions related to a specific memristor.

In 2021, Li et al. built a memristor synapse-coupled neural network by coupling neurons with the proposed LAM. By controlling the coupling strength, they study coexisting multiple firing patterns under different initial conditions, such as periodic and chaotic bursting [58]. In 2023, Lai et al. constructed a neural network model using discrete LAM. This model can generate co-existing heterogeneous attractors [59]. In 2024, Chen et al. constructed a bineuron model by bidirectionally connecting an LAM between two neuron models. Under different memristor control parameters, complex spiking/bursting activities and their transitions are revealed [60]. Hu et al. proposed an extensible LAM as a coupling synapse between two neurons. Taking the coupling strength and the initial state of the memristor synapse as controllable variables, they reveal various synchronization phenomena triggered by the introduced memristor [61].

Synapses simulated with LAMs can generate more complex dynamics behaviors, enriching the

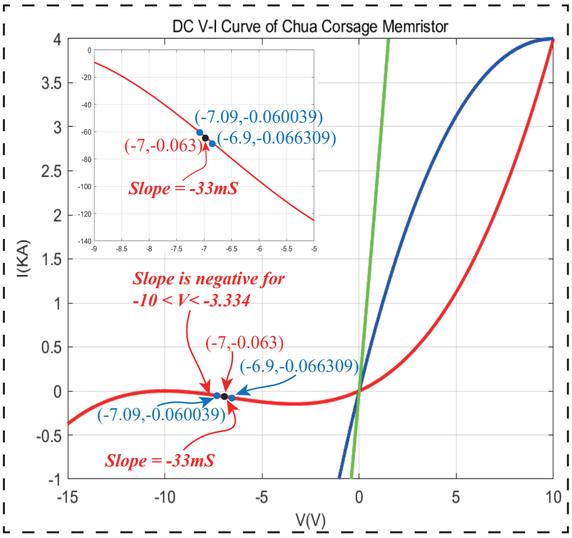

Fig. 4 DC V–I curve of the Chua Corsage Memristor

research content in the field of memristive neural networks.

2.2.6 Challenges of Memristive Synapses

Memristors can effectively implement synapses. For example, large conductance tuning range can achieve richer plasticity regulation, volatile and non-volatile can achieve STP and long-term plasticity, and fast switching speed can achieve rapid response of synapses. However, their practical applications still face several challenges.

At first, although memristors possess a relatively large range of conductance, this range cannot be easily converted into many distinguishable conductance levels due to random performance fluctuations and noise limitations, which reduces the precision of memristors. Therefore, in the design of memristors, it is essential to select a low-noise material and improve the consistency and reliability of the device.

Second, external environmental factors can affect the stability of memristors and reduce their usage time. It is essential to thoroughly consider the intrinsic stability of materials and enhance the device's resistance to environmental interference through optimized packaging processes.

Third, current memristors are unable to fully emulate synaptic functions, such as BTSP and homeostatic plasticity, and most lack adaptive learning mechanisms. Therefore, device innovations are necessary to mimic biological synapses more fully.

Finally, although various mathematical synaptic memristor models are available for dynamics analysis, the lack of corresponding devices has confined them to the theoretical analysis stage.

2.3 Transistor-based synapse

Novel transistors can simulate synaptic function by changing channel conductance and have advantages such as high stability, low power consumption, multi-modal control [62], and multi-stimulus response [63]. According to the working principles, transistor-based synapses can be divided into four types: floating-gate transistors (FGTs), electrolyte-gated transistors (EGTs), ferroelectric field-effect transistors (FeFETs), and optoelectronic transistors (OETs). A comparison of various types of synaptic transistors is presented in Table. 2.

2.3.1 Floating-Gate Transistors

The structure of FGTs is similar to that of traditional metal-oxide-semiconductor field-effect transistors (MOSFETs), but with the incorporation of an additional floating gate. In traditional FETs, the charges accumulated in the channel dissipate quickly after the gate voltage is removed, resulting in volatility. FGTs employ a dielectric layer to isolate the floating gate from the channel. The charges injected into the floating gate can be trapped without external voltage. The presence of these stored charges alters the effective threshold voltage of the device, thereby persistently modulating channel conductance [64].

In 2019, Paul et al. designed a floating-gate synaptic device based on MoS_2 structure. This device successfully simulates the behavior of synaptic weight update, symmetric and asymmetric STDP [65]. To improve the precision of synaptic operations, it is necessary to ensure the linearity and symmetry of weight updates. In 2023, Cho et al. proposed a van der Waals heterostructure-based double-floating-gate synaptic transistor. This device enhances the linearity, symmetry, and dynamic range of synaptic weight updates through double tunneling barriers and floating gates for charge redistribution. It can achieve EPSC, SRDP, STDP, LTP, and LTD [66].

Furthermore, flexible electronic devices are gaining increasing importance in practical application scenarios. In 2024, Zhu et al. proposed a synaptic transistor for flexible electronic devices using $Ti_3C_2T_x$ as the floating gate and carbon nanotubes as the channel. This device demonstrates precise synaptic weight modulation, PPD, and PPF [67].

FGTs have the advantages of high stability, long-term retention, and CMOS compatibility. However, they also face challenges such as high operating voltage, poor biological plausibility, and size reduction.

2.3.2 Electrolyte-Gated Transistors

EGTs use electrolyte materials containing mobile ions as the gate dielectric layer, exploiting ion migration to modulate channel conductance. According to the working principle, EGTs can be sorted into two categories : 1) electrostatic modulation, where ions in the electrolyte do not penetrate into the semiconductor and form an electric double layer (EDL) at the interface. 2) electrochemical modulation, which allows ions to penetrate into the semiconductor.

In 2018, Yang et al. proposed an EDL transistor based WO_3 and ionic liquid, N,N-diethyl-N-(2-methoxyethyl)-N-methylammonium bis-(trifluoromethylsulphonyl)-imide (DEME-TFSI). Electrolyte gating can alter the transport characteristics of WO_3 and simulate the dynamics of Ca^{2+}. The transistor successfully realizes STP, LTP, PPF, and STDP [68]. Organic semiconductors have emerged as frontier materials for electronic devices, leveraging their unique advantages such as low cost, chemical structural diversity, flexibility, and processability. In 2022, Liu et al. developed a vertical organic EDL transistor based on poly(3-hexylthiophene) (P3HT) and ionic liquid, 1-ethyl-3-methylimidazolium bis(trifluoromethylsulfonyl)imide (EMIM: TFSI). This synaptic transistor can simulate STP, PPF, LTP, and LTD, and it has multiple sensing and response functions to simulate human perception [69]. In 2024, Zhu et al. proposed a flexible organic electrochemical transistor based on poly[(bithiophene)-alternate-(2,5-di(2-octyldodecyl)- 3,6-di(thienyl)-pyrrolyl pyrrolidone)] (DPPT-TT) and poly(methyl methacrylate) (PMMA)/$LiClO_4$. Even after bending, the device's electrical performance remains stable. It can achieve EPSC, PPF, STP, and LTP [70].

EGTs exhibit unique advantages in emulating synaptic functions, such as low-voltage operation, flexible structure, and multimodal signal processing capabilities. But they also have inherent limitations, including vulnerability to environmental interference, insufficient stability, and high integration difficulty.

2.3.3 Ferroelectric Field-Effect Transistors

The most significant difference between FeFETs and MOSFETs lies in the replacement of the SiO_2 gate insulator with a ferroelectric material that exhibits a high dielectric constant. FeFETs leverage the polarization properties of the ferroelectric layer to alter carrier concentration and modulate channel conductance.

In 2017, Jerry et al. demonstrated a FeFET based on $Hf_{0.5}Zr_{0.5}O_2$ and Si. The fabricated device exhibits the symmetric potentiation and depression characteristics of the synapses [71]. It is crucial to use FeFETs to achieve flexible artificial synapses. In 2022, Xia et al. fabricated a ferroelectric synaptic transistor based on carbon nanotubes (CNTs) and $HfO_2/AlO_x/HfO_2$. This device has extremely high flexibility and can achieve PPF, PPD, LTP, and LTD [72]. 2D materials, with intrinsic advantages such as atomic thickness and high carrier mobility, can significantly reduce the power consumption of transistors and improve response speed. In 2024, Song et al. presented 2D FeFETs based on nanoscale $HfZrO_2$ and 2D SnS_2. The fabricated device demonstrates multilevel data storage capabilities, fast response (1 μs), and successfully emulates EPSC, IPSC, PPF, and STDP [73].

FeFETs exhibit several promising features, including large on/off ratios, non-destructive readout, precise control of channel conductance, and rapid response. However, they also have risks of polarization fatigue and large leakage current.

2.3.4 Optoelectronic Transistors

Optoelectronic synapses can optically simulate synaptic plasticity. There are usually two working mechanisms, photogenerated carrier transport and photoinduced chemical reactions. The materials of OETs include oxide semiconductors, perovskite, and some 2D materials.

Table 2 Comparison of different types of transistors.

Type	Channel	Function	Energy	Ref
FGTs	MoS_2	STDP	5fJ	[65]
	MoS_2	SRDP, STDP, LTP, LTD	–	[66]
	Carbon Nanotube	PPF, PPD	5.3fJ	[67]
EGTs	WO_3	STP, LTP, PPF, STDP	36pJ	[68]
	P3HT	STP, PPF, LTP, LTD	0.06fJ	[69]
	DPPT-TT	PPF, STP, LTP	2.08fJ	[70]
FeGTs	Si	potentiation, depression	98.01mJ	[71]
	CNTs	PPF, PPD, LTP, LTD	–	[72]
	SnS_2	PPF, STDP	48aJ	[73]
OETs	IGZO	PPF, PPD, STM-LTM	–	[74]
	IGZO/$CsPbBr_3$	EPSC, PPF, LTP, IPSC, STP-LTP	1.35pJ	[75]
	ReS_2	EPSC, STM-LTM	2.5pJ	[76]

Table 3 Comparison of memristor and transistor.

Type	Energy	Size	Complexity	Precision	Stability	Switching speed	On/Off ratios
Memristor	✓	✓	✓			✓	✓
Transistor				✓	✓	✓	✓

Note: ✓ represents the better one.

The photo-generated carrier trapping effect at the semiconductor-dielectric interface can be used to regulate OETs. In 2018, Wu et al. designed a transistor that combines photonic and electric stimulus based on the inherent persistent photoconductivity of indium–gallium–zinc oxide (IGZO) thin films. This transistor can achieve PPF, STM-LTM under the ultraviolet light stimulus, and PPD under the electrical stimulus [74]. Perovskite materials possess high optical absorption coefficients and high mobility, showing great promise in OETs. In 2021, Xin et al. designed an IGZO OETs embedded with $CsPbBr_3$ QDs. The device achieves optically tunable EPSC, PPF, STP-LTP, and electrically stimulated IPSC [75]. 2D materials enable high-density integration, and carrier trapping and de-trapping at the dielectric interface can facilitate optoelectronic synapses. In 2024, Chen et al. introduced a wrinkled ReS_2 transistor. This optoelectronic synapse achieves light-modulated EPSC, STM-LTM, and updates conductance state to up to 8-bit linear and symmetric values [76].

OETs can solve hardware redundancy caused by the isolation of neuromorphic computing and sensors in traditional artificial synapses. Furthermore, OETs use light to regulate synaptic function, which can combine visual systems with brain function, showing great potential in the fields of visual information perception, memory, and processing. However, there are also several limitations, including a limited light response wavelength and difficulty in achieving the inhibitory and other complex functions of synapses.

Memristors-based synapses and transistors-based synapses have different physical mechanisms and application scenarios. Their comparison is shown in the Table. 3. Except for common usage scenarios, memristors are suitable for in-memory computing due to their size and power consumption, transistors are suitable for biomedical sensors and hybrid neuromorphic hardware due to their precision and stability.

3 Neuron Model

Neuron models are abstract and mathematical descriptions of biological neurons, which can be used to simulate the functions and activities of neurons in neural networks.

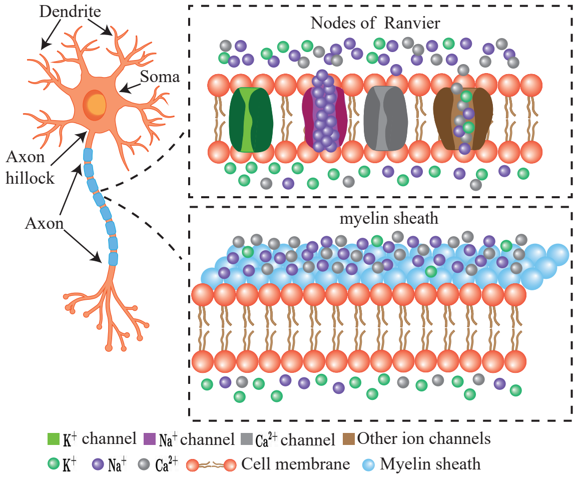

Fig. 5 The physiological structure of neuron.

3.1 The Basic Structure of Neurons

As shown in Fig. 5, a typical neuron can be divided into three functionally distinct parts: soma, dendrites, and axons. Soma consists of the nucleus, cell membrane, and cytoplasm. The nucleus mainly stores genetic material and provides gene codes for protein synthesis, but does not directly participate in the generation and transmission of neuronal signals. The cytoplasm is the primary site for metabolism, where the major chemical reactions occur. Dendrites and axons are two types of synapses. Dendrites are responsible for receiving signals, while axons transmit signals. The axon hillock is located between the soma and the axon. Myelin sheaths typically appear in vertebrates and some copepods. They wrap around most axons, leaving only certain sections exposed, forming Ranvier nodes [77]. The region between the axon hillock and the beginning of the myelin sheath has been recognized as the site of AP generation [78]. Because ion exchange only occurs at the Ranvier nodes, signal transmission in myelinated neurons occurs in a saltatory manner, resulting in extremely fast transmission speeds. Furthermore, myelination is a progressive process that is closely associated with the development and function of the brain [79].

3.2 Generation of Action Potential

APs are closely related to the ion channels on the cell membrane, and the generation process is shown in Fig. 6. When a neuron receives an excitatory stimulus, the membrane potential in the axon hillock increases. Once it reaches the threshold of Na^+ channels, these channels are rapidly activated. Due to the concentration gradient of ions inside and outside the cell, the massive influx of Na^+ leads to neuronal depolarization. The membrane potential then rises to the threshold of K^+ channels, which leads to a large efflux of K^+, causing neuronal repolarization, and a single AP is completed. The depolarization of the AP propagates to adjacent regions through local currents, which activate new Na^+ channels, repeating the above process and triggering new APs until the signal is transmitted to the axon terminal. When receiving an inhibitory stimulus, the neuron hyperpolarizes, and the membrane potential decreases to the threshold of Ca^{2+} channels, allowing a large influx of Ca^{2+}. This results in an increase in the membrane potential and the activation of Na^+ channels, then repeating the ion flow process similar to an excitatory stimulus.

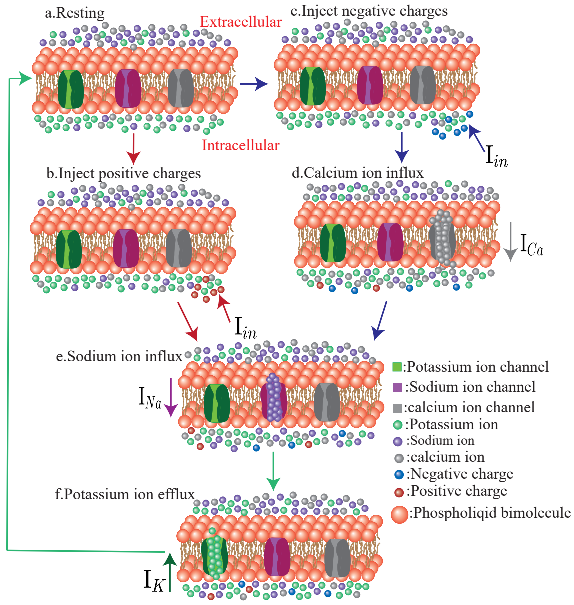

Fig. 6 The firing process of neurons. a) Resting state; b) Injecting positive charges; c) Injecting negative charges; d) Ca^{2+} influx; e) Na^+ influx; f) K^+ efflux. EPSP: a-b-e-f-a, IPSP: a-c-d-e-f-a.

3.3 The Development of Neuron Models

Integrate-and-Fire (IF): In 1907, Lapicque proposed the IF neuron model and compared it with the data obtained from experiments on stimulating the sciatic nerve of frogs. The IF model suggests that the cell membrane can be simulated using a capacitor and a resistor, which lays the foundation for future neuron models [80].

Leaky Integrate-and-Fire (LIF): In the 1950s, Lilly improved the IF model by adding a linear leak resistor, making it more consistent with the physiological properties of cell membrane [81]. Due to its simplicity in structure, it is suitable for large-scale neural networks.

Hodgkin-Huxley (HH): In 1952, Hodgkin and Huxley conducted experiments on the giant axon of the squid and identified three different types of ion current. They derived the HH model and modeled it using an equivalent circuit [82]. The biological plausibility enables it to achieve various firing behaviors.

Current neuron models can be classified into three main categories: variants of HH model, variants of the LIF model, and other models. The variants of the LIF model are non-conductance-dependent, focusing mainly on the integration of membrane potential without considering specific ion channels. In contrast, the variants of the HH model are primarily conductance-dependent, they replicate neuronal dynamics by simulating ion channels and currents. The different models are shown in Table. 4.

3.3.1 LIF Model's Variants

Quadratic Integrate-and-Fire (QIF): In 2000, Latham introduced a quadratic term in membrane potential, which is the same as the previously proposed θ-neuron model [83, 84], to study the dynamics of the neural network under low firing rate [85]. This model is more closely aligned with the actual AP process of neurons.

Integrate-and-Fire-or-Burst (IFB): In 2000, Smith proposed the IFB model to simulate relay neurons in the lateral geniculate nucleus of the cat's thalamus. By adding a low threshold Ca^{2+} variable, this model achieves dual thresholds of bursting and tonic spiking [86]. The simplicity of this model can make it a candidate for large-scale simulations of thalamic neural networks.

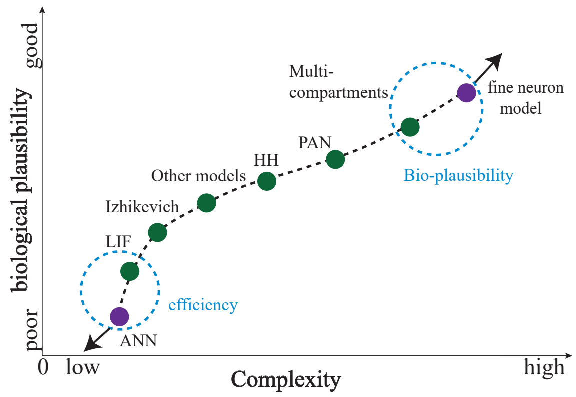

Fig. 7 Exploring the relationship between the biological plausibility of neuronal models and their complexity is crucial. The two dashed circles indicate two significant research directions: enhancing biological plausibility and minimizing complexity.

Resonate-and-Fire (RF): In 2001, Izhikevich introduced the RF model to explain how subthreshold oscillations affect neuronal spike dynamics [87]. Although similar to the IF model, the RF model exhibits distinct dynamics, including damped oscillations and resonance.

Exponential Integrate-and-Fire (EIF): In 2003, Fourcaud-Trocme proposed the EIF model by approximating Na^+ activation variables near the threshold with an exponential function [88]. This model can accurately predict the response of neurons to high-frequency inputs.

Spike Response Model (SRM): In 2003, Jolivet proposed SRM, which is a generic threshold model of IF. This model can reliably predict the spiking time, membrane potential, average firing rate, and coefficient of variation of the interspike interval (ISI) distribution [89]. Compared to the IF model, SRM has time-dependent thresholds and more realistic after-hyperpolarized potential, and it is often used in spiking neural networks (SNNs) algorithms.

adaptive Exponential Integrate-and-Fire (aEIF): In 2005, Brette and Gerstner combined the EIF model with Izhikevich's reset-based adaptive equations to construct the aEIF model [90]. This model accurately predicts the firing sequences of regular spiking (RS) neurons and is applicable to large-scale cortical networks.

3.3.2 HH Model's Variants

FitzHugh-Nagumo (FHN): In 1961, FitzHugh proposed the Bonhoeffer-van der Pol (BVP) model, which corresponded well to the HH model [91]. In 1962, Nagumo implemented an equivalent circuit of the BVP model using tunnel diodes [92]. The 2D FHN model is more straightforward and more amenable to analysis compared to the 4D HH model.

Connor-Stevens: In 1971, Connor and Stevens incorporated A-type transient K^+ channels into the HH model to explain the repetitive firing of gastropod neurons [93, 94].

Morris-Lecar (ML): In 1981, Morris and Lecar developed the 3D ML model using K^+ and Ca^{2+} conductances to investigate the complex oscillatory behavior in barnacle muscle fibers. They later simplified the original equations to a 2D model [95]. The ML model is simple, yet capable of generating rich firing behaviors.

Hindmarsh and Rose (HR): In 1984, Hindmarsh and Rose developed the HR model, an enhancement of the FHN model. This model incorporated three key variables: membrane potential, recovery variable, and slow regulated current, to account for the firing patterns observed in snail neurons [96, 97]. They subsequently analyzed thalamic neurons as well [98, 99]. The HR model is effective in explaining neuronal bursting behavior.

Chay: In 1985, Chay constructed a 3D nonlinear system consisting of membrane potential, probability of opening voltage-dependent K^+ channel, and intracellular concentration of Ca^{2+} to simulate chaotic phenomena in specific cardiac cells and pancreatic β cells [100]. This is the first simple and biologically plausible model of neuronal chaos.

Wilson: In 1999, Wilson proposed a new and simple approximation of the dynamics of neocortical neurons based on four ion currents: Na^+ current, K^+ current, low threshold Ca^{2+} current and slow afterhyperpolarizing K^+ current [101]. The Wilson model can exhibit four different firing modes at different parameter values: RS, fast-spiking, continuously bursting, and intrinsic bursting.

Izhikevich: In 2003, Izhikevich proposed a simple spiking model that combined the biological plausibility of the HH model with the computational efficiency of IF model [102]. By tuning the parameters, this model could replicate the spiking and bursting behavior of cortical neurons.

W-Z: In 2015, Wang and Zhang proposed the W-Z model considering the self-induction effect of ion currents, and further demonstrated that the general trends in membrane potential and energy consumption in this model align with the HH model and the experimental neurophysiological results [103, 104]. W-Z model contributes to the correct understanding of energy consumption in neuronal activities.

Power-Adaptive Neuron (PAN): The HH model only describes the dynamics of the ion channels, lacking descriptions of neuronal growth processes, adaptive energy consumption, and adjustment in firing rates. In 2024, Li et al. designed PAN model with power-adaptive adjustment capability considering the function of myelin sheaths [105].

3.3.3 Other Models

Rate: Rate model, which first appears in the 1930s, can be seen as an extension of the Lotka-Volterra model (used to describe interspecies competition in ecosystems). It describes neuronal activity based on the average firing rate without considering the internal details of individual neurons [106]. The Rate model helps improve understanding of selection mechanisms in the neural system and facilitates the construction of computational models for cognitive and motor functions.

McCulloch-Pitts (MP): In 1943, McCulloch and Pitts proposed the MP model based on the all-or-none property of neurons [107]. It is the first computational model of artificial neurons designed to describe the fundamental computational principles of biological neurons.

Wilson-Cowan: In 1972, Wilson and Cowan proposed the Wilson-Cowan mathematical model to explain the interactions between neuronal populations in the brain [108]. This model serves as a simple approximation for the more complex structures of the brain's neocortex and associated thalamic nuclei.

Oscillators: Oscillators can generate oscillations similar to neuronal activity [109] and there are various oscillation models, such as RLC oscillator [110, 111] and RC oscillator [112–114].

Maps: These models use mappings to describe the electrical activity of neurons, such as Cazelles map [115], Rulkov map [116], Chialvo map [117], and Zandi map [118], etc. Extensive researches have shown that the these models can generate rich nonlinear dynamics behaviors.

Neuron models can be evaluated from two aspects: complexity and biological plausibility, as illustrated in Fig. 7. Their representatives are the simplified LIF model and the fine HH model, respectively. Simplified model nodes have limited computing power, while fine models have high complexity. Therefore, the design of high computing power fine neural node circuits that are easy to implement has gradually become a trend.

3.4 The Firing Patterns

Different types of neurons exhibit distinct firing patterns, which allow them to encode and process information in various situations, achieving a range of complex physiological functions [119]. Numerous firing patterns have been achieved [120, 121].

All-or-nothing firing: This is a basic principle of all neurons. Neurons only fire when they reach a threshold, otherwise they slowly return to resting. It can convey discrete information [122].

Refractory period: After APs, neurons temporarily lose or decrease their response to stimuli for a period of time. It can be divided into relative and absolute refractory periods. This phenomenon ensures the unidirectional conduction of neuronal electrical signals and prevents excessive excitation of neurons.

Tonic spiking: Neurons fire continuously and regularly. It represents the duration of stimuli [123].

Tonic bursting: Neurons burst continuously and repeatedly. It may be related to the generation of some forms of synchronized rhythmic oscillations of sleep and of epileptic seizures [124].

Phasic spiking: Neurons produce a brief AP, followed by a resting state or a longer period of low activity. It can detect the beginning of stimuli.

Phasic bursting: Neurons continuously release a series of APs, and then enter a relatively inactive period.

Spike latency: Neurons fire spikes with a delay. In sensory systems, different neurons can utilize spike latencies to encode information [125, 126].

Accommodation: Neurons do not fire under slowly increasing stimuli. This mechanism can filter stimuli and reduce the energy consumption of neurons.

Mixed mode: Neurons exhibit both bursting and firing. This characteristic involves certain dependent ion channels.

Bistability: Neurons are able to exist stably in two different membrane potential states (such as resting and firing) and achieve state switching through brief stimuli under specific conditions, which require the involvement of a non-voltage-gated K^+ channel.

Spike frequency adaptation: Under continuous stimuli, the firing frequency of neurons gradually slows down over time. It may be related to Ca^{2+} activated Cl^- channel [127] and helps extract signals at different time scales [128].

Class 1 excitability and Class 2 excitability: The firing frequency of class 1 excitability increases from 0 to a non-zero value gradually, whereas it switches from 0 to a nearly fixed value rapidly for class 2 excitability. M-type K^+ currents and inhibitory autaptic currents can induce the transition from class 1 excitability to class 2 excitability. The increase of A-type K^+ conductance, the decrease of Ca^{2+} conductance and excitatory autaptic current induce the opposite transition [129].

Subthreshold oscillations: Periodic fluctuations in neuronal membrane potential when no AP is generated. This oscillation is a rhythmic activity generated by the dynamic balance of ion channels, which is of great significance for the signal integration, rhythm generation, and network synchronization of neurons [130].

Resonator: Neurons exhibit strong responses to stimuli within a specific frequency range, indicating that neurons have frequency selectivity.

Integrator: Neurons accumulate current or voltage stimulus in time and space, firing when reaching the threshold.

Rebound spiking and Rebound bursting: After experiencing hyperpolarization, neurons fire or burst when their membrane potentials return to resting levels or further depolarize. This may be related to the influx of Ca^{2+} during hyperpolarization.

Threshold variability: Neurons have a variable threshold that depends on the prior activity of the neurons.

Table 4 The development of neuron model.

Model	Object	Formula
LIF (1950s)	Improvement of IF model	$RCV' = IR - (V - V_r)$ if $V \geq V_{\text{thresh}},$ then $V \leftarrow c$
HH (1952)	Giant axon of squid	$CV' = I - g_{Na}m^3h(V - V_{Na}) - g_K h^4(V - V_K) - g_L(V - V_L)$
FHN (1961)	Van der Pol's equation	$V' = c[u + (1 - a^2)V + aV^2 + V^3/3]$ $u' = -(V + bu)/c$
ML (1981)	Barnacle Muscle Fiber	$CV' = I - g_L(V - V_L) - g_{ca}M_\infty(V)(V - V_{ca}) - g_K N(V - V_K)$ $\frac{dN}{dt} = \lambda_N(V)\left(N_\infty(V) - N\right)$
HR (1984)	Thalamic neuron	$V' = u - aV^3 + bV^2 + I - w$ $u' = c - dV^2 - u$ $w' = r(s(V - V_1) - w)$
Chay (1985)	Cardiac myocyte	$V' = -g_I m_\infty^3 h_\infty(V - V_I) - g_{K,V}h^4(V - V_K) - g_{K,Ca}\frac{C}{1+C}(V - V_K) - g_L(V - V_L)$ $\frac{dn}{dt} = \frac{[n_\infty - n]}{\tau_n}$ $\frac{dC}{dt} = \rho\left\{m_\infty^3 h_\infty(V_C - V) - k_C C\right\}$
QIF (2000)	Neural networks in low firing rate	$CV' = \frac{(V - V_r)(V - V_T)}{R(V_t - V_r)} + I$ if $V = V_{\text{peak}},$ then $V \leftarrow V_{\text{reset}}$
IFB (2000)	Cat thalamic relay neuron	$CV' = I - I_L - g_{\mathrm{T}}H(V - V_h)h(V - V_{\mathrm{T}})$ $\frac{dh}{dt} = \begin{cases} -h/\tau_h^- & (V > V_h) \\ (1 - h)/\tau_h^+ & (V < V_h) \end{cases}$ if $V = V_{\text{thresh}},$ then $V \leftarrow V_{rest}$
RF (2001)	Similar to LIF	$z' = I + (b + iw)z$ if $\mathrm{Im} z = 1,$ then $z \leftarrow z_0$
Rulkov (2001)	Bursting neuron	$x_{n+1} = \frac{\alpha}{1 + x_n^2} + y_n$ $y_{n+1} = y_n - \sigma x_n - \beta$
Izhikevich (2003)	Cortical neuron	$V' = 0.04V^2 + 5V + 140 - u + I$ $u' = a(bV - u)$ if $c \geq 30$ mV, then $\begin{cases} V \leftarrow c \\ u \leftarrow u + d \end{cases}$
EIF (2003)	Cortical neuron	$CV' = -g_L(V - V_r) + g_L\Delta_T \exp\left(\frac{V - V_T}{\Delta_T}\right) + I$ if $V \geq V_{\text{thresh}},$ then $V \leftarrow V_r$
SRM (2003)	Generic threshold model of IF	$u(t) = \eta(t - \hat{t}) + \int_{-\infty}^{+\infty} \kappa(t - \hat{t}, s)I(t - s)\,ds$ if $u(t) \geq \theta$ and $\dot{u}(t) > 0,$ then $\hat{t} = t$ $\theta(t - \hat{t}) = \begin{cases} +\infty & \text{if } t - \hat{t} \leq \gamma_{ref} \\ \theta_0 + \theta_1 \exp(-(t - \hat{t})/\tau_\theta) & \text{else} \end{cases}$
aEIF (2005)	RS pyramidal neuron	$CV' = -g_L(V - V_r) + g_L\Delta_T \exp\left(\frac{V - V_T}{\Delta_T}\right) - w + I$ $\tau_{\mathrm{w}}\frac{dw}{dt} = a\left(V - V_{\mathrm{L}}\right) - w$ if $V = V_{\text{peak}},$ then $V \leftarrow V_{\mathrm{r}}$
W-Z (2015)	Neuronal activity energy model	$U_m = r_{0m}I_{0m} + r_{1m}I_{1m} + L_m\dot{I}_{1m}$ $I_{0m} = I_{1m} - I_m + \frac{U_{im}}{r_m} + C_m\dot{U}_{0m}$ $U_{im} = C_m r_{3m}\dot{U}_{0m} + U_{0m}$
PAN (2025)	HH model and myelin sheath	$V' = I - g_{Na}(V - V_{Na}) - g_K(V - V_K) - g_{Ca}(V - V_{Ca}) - g_A(V - V_A) - g_T(V - V_T)$

Inhibition-induced spiking and Inhibition-induced bursting: Neurons fire or burst under sustained inhibitory input. This may be related to sustained activation of the Ca^{2+} channels.

Depolarizing after-potential (DAP): After AP repolarization, the membrane potential briefly remains at a level that is more depolarized than the resting potential. It may enhance neuronal excitability and even trigger repetitive firing.

Excitation block: Although neurons are stimulated to a threshold, they are unable to generate or transmit APs. This may be related to abnormal ion channel function, synaptic transmission imbalance, and insufficient energy metabolism.

Dysfunctional Ca^{2+} channel: It is mainly caused by the dysregulation of Ca^{2+} channels and leads to abnormal firing of neurons.

Chaos: Neuronal firing activity exhibits complex, non-periodic, and highly sensitive behavior to initial conditions.

3.5 Energy Description of Neural Circuit

Neurons consume energy when firing APs. Different external stimuli can cause changes in their firing patterns and energy, and neural coding is also closely related to energy consumption [131]. Therefore, energy description is crucial for neural circuit. Sarasola et al. proposed the Hamilton energy function using Helmholtz's theorem, which can be used to describe the energy of neural models [132]. Through scale transformation, the Hamilton energy function of the neural circuit is equivalent to the field energy function [133]. Its specific content is as follows [134].

Considering a general continuous autonomous dynamical system represented by

$$\frac{dx}{dt} = f(x) \tag{6}$$

The velocity vector field $f(x)$ can be regarded as a sum of two vector fields, as follows

$$f(x) = f_c(x) + f_d(x) \tag{7}$$

where $f_c(x)$ is the conservative field containing the full rotation, $f_d(x)$ is the dissipative field containing the divergence.

The dynamical equations can also be expressed in a generalized Hamiltonian form,

$$\frac{dx}{dt} = [J(x) + R(x)]\,\nabla H \tag{8}$$

where $J(X)$ is a skew-symmetric matrix, $R(x)$ is a symmetric matrix, ∇H is the gradient vector of a smooth energy function $H(x)$.

Then the Hamilton energy function satisfies the following equation:

$$\begin{aligned} &\frac{dH}{dt} = \nabla H^T R(x) \nabla H = \nabla H^T f_d(X) \\ &\nabla H^T J(x) \nabla H = 0 = \nabla H^T f_c(x) \end{aligned} \tag{9}$$

the superscript T means a transpose operation of matrix.

Hamiltonian energy can study the neuronal firing behaviors [135–139], the effect of external stimulus on neuronal firing behaviors [140, 141], energy exchange and synchronization between coupled neurons [142, 143], and estimate stochastic resonance and inverse stochastic resonance [144].

As a mathematical neuron model, HR model can reproduce the main properties of neuronal activities and is commonly used for energy analysis. In 2006, Torrealdea et al. defined the Hamilton energy function of HR neurons and estimated the energy consumption of neurons in different firing patterns [138]. In 2015, Song et al. renewed Hamilton energy function and clarified the dependence of energy consumption on external forcing current in a directional way. They also indicate that when neuron is bursting or chaotic, the energy function is low [139]. The fluctuation of neuron membrane potential can alter the distribution of electromagnetic field inside and outside the neuron. Thus, the influence of electromagnetic induction on the membrane potential should be considered and it can be achieved through flux-controlled memristors [145, 146]. In 2019, Usha et al. considered electromagnetic induction and demonstrated that the negative feedback in Hamilton energy function effectively stabilizes the chaotic trajectories and controls the phase space [141]. In 2023, Lu et al. verified that Hamiltonian energy is practicable to study the energy dissipation of neuron in different oscillation states and the synchronization phenomenon of coupled HR model [143].

3.6 Memristive Neural Circuits and Applications

Neural circuits can be applied to signal processing [147–149], neuromorphic computing [150], and electrical signals drive the electromechanical arms and legs [112, 151, 152]. Memristors have become promising devices for neural circuits, as shown in Table. 5.

Memristors and capacitors constitute the main modules in the LIF neuron model, and the integration and firing processes are achieved through the charging and discharging of the capacitors controlled by memristors. In the HH model, memristors are often used to simulate ion channels [153].

For physical devices, in 2021, Wang et al. designed a lobula giant movement detector neuron based on Ag/few-layer black phosphorous (FLBP)-$CsPbBr_3$/ITO. This circuit can simulate the integration process, refractory period, light-modulated spiking frequency of neuron, encode optical input and achieve collision avoidance function of the robot car [147]. In 2023, Yan et al. constructed LIF model based on TiN/HfO_2/IGZO/Si memristor and the integration process, intensity-modulated spiking frequency were simulated. They further construct SNNs to achieve spatiotemporal model recognition and unsupervised synaptic weight update function [150]. In 2024, Shan et al. constructed LIF model based on Au/Ta_2O_5:Ag/ITO memristor. This circuit realizes wavelength-modulated spiking frequency and color recognition function [148].

In 2018, Yi et al. designed a scalable nanoscale VO_2 active memristor to mimic the ion channels in HH model. This circuit can achieve 23 distinct firing behaviors [55]. In 2022, Xu et al. reported an HH retina circuit with adaptive VO_2 memristors. This circuit achieves refractory period, tonic bursting, tonic spiking of neuron and light-adaptable functions of the biological visual perception system [149]. In 2025, Yang et al. developed a universal HH model based on NbO_x memristor, investigated 23 firing behaviors and discussed potential applications of different firing behaviors in neuromorphic intelligence systems [119].

For mathematical model, the design of memristors is more flexible and has a wider range of applications. In 2024, Li et al. proposed an improved HH model and achieved 24 different firing

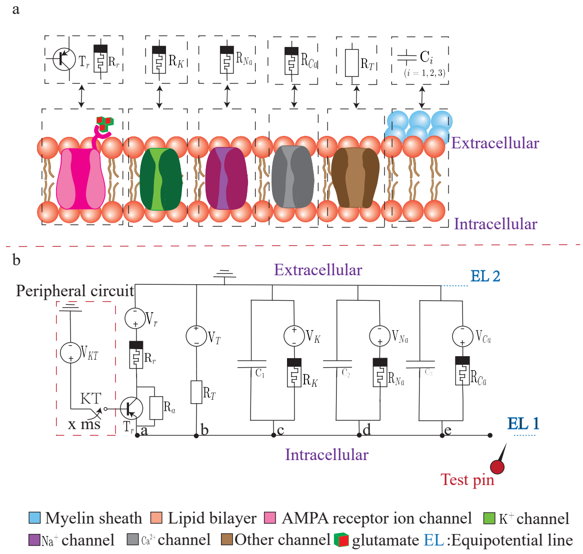

Fig. 8 Biological alternatives and hardware circuits. (a) Corresponding electronic components as cell organelles; (b) Adaptive biomimetic neuronal circuits.

patterns [120]. Subsequently, they explore myelin sheaths in neurons [154] and design PAN model based on the functions of myelin sheaths [105], as shown in Fig. 8. They further incorporate synaptic and myelin plasticity in neurons and design the corresponding circuits [155]. In 2025, Sun et al. designed an algal light sensing circuit and constructed intelligent optical sensor array to realize spiking camera [10]. Guo et al. presented a simple neural circuit to drive an electromechanical arm device by activating Ampere's force via the load circuit adhered to the moving beam, and the load circuit is coupled with the neural circuit for energy conversion [151].

When designing neural circuits, the following issues are worth considering:

1): The neural circuits used in sensory sensors have relatively single functions. For example, while the human eye can simultaneously perceive information such as obstacles, colors, and brightness, sensors usually only capture one type of information. Besides, multimodal fusion is also essential.

2): The power consumption of most neural circuits is much higher than that of biological neurons, and methods to reduce power consumption still need to be researched.

Table 5 Comparison of neuron models with different memristors.

Model	Structure	Firing	Energy	Application	Ref
LIF	Ag/FLBP-$CsPbBr_3$/ITO	Integration process, Refractory period, Light-modulated spiking frequency	2.1nJ	Biomimetic compound eye	[147]
	TiN/HfO_2 /IGZO/Si	integration process, intensity-modulated spiking frequency	32.65fJ	SNNs	[150]
	Au/Ta_2O_5:Ag /ITO	integration process, wavelength-modulated spiking frequency	–	Color photoreceptor	[148]
HH	Pt/VO_2/Pt	23 types	5.6fJ	–	[55]
	Ti/Au/VO_2/Si /SiO_2	refractory period, tonic bursting, tonic spiking	–	Retina	[149]
	Ti/NbO_x/Pt	23 types	29pJ	–	[119]

3): Neural circuits also need to consider their robustness against external interference and their consistency with the processing mechanisms of biological neurons.

3.7 Dynamics Analysis

Different mathematical memristors have been proposed for dynamics analysis of FHN [156–158], ML [159–161], HR [162–164], Rulkov [165–167], Wilson models [168–170], and their improved model. These researches have analyzed firing patterns, synchronization, energy control, and electromagnetic radiation of memristive neurons. Dynamics phenomena such as periodic firing, periodic bursting, chaotic bursting, folding bursting, period-chaos transfer, and hyperchaotic firing have been discovered.

LAMs have advantages in simulating neuronal behaviors [40–42] and have been widely discussed. In 2020, Dong et al. presented a bistable nonvolatile LAM [171]. In 2023, Zhang et al. proposed a novel memristive autapse-coupled neuron model using a LAM as an autapse and simultaneously introducing a flux-controlled piecewise-nonlinear memristor to describe the external electromagnetic radiation. It can exhibit rich and complex hidden firing dynamics and homogeneous multistability [172]. Ying et al. constructed second-order and third-order neuronal RC circuits exhibiting 21 different firing behaviors based on VO_2 LAM, and revealed firing behaviors emerge on or near the edge of chaos [173]. In 2025, Shao et al. constructed RC neural circuit having the class I excitability and the class II excitability, and investigated synchronization between coupled neurons [113].

Conducting dynamics analysis on neural circuits help to understand the working mechanisms of the brain [173] and the potential mechanisms underlying the occurrence of diseases [146, 174]. The chaotic phenomenon of neural circuits can be be applied to secure communication [175] and image encryption [176].

4 Memristive Neural Networks

4.1 Artificial Neural Networks

Since 1958, artificial neural networks (ANNs) have undergone a tortuous and lengthy development [177–179]. The calculation process of an artificial neuron can be written by

$$y = f\left(\sum_{i=0}^{N} w_i x_i + b\right) \tag{10}$$

where x_i is the input of neuron and y is the output, w_i is the weight, b is the bias, and $f(x)$ is nonlinear activation function.

The current ANNs include convolutional neural networks (CNNs), recurrent neural networks (RNNs), feedforward neural networks (FNNs), and most of them are deep neural networks (DNNs). ANNs learning paradigms are divided into supervised learning, unsupervised learning, semi-supervised learning and reinforcement learning.

In supervised learning, the network is continuously trained and adjusted using inputs and

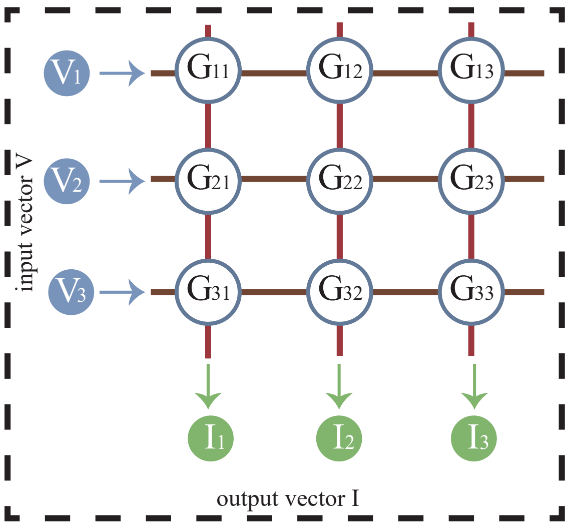

Fig. 9 VMM based on memristor crossbar array.

corresponding labels (i.e., expected outputs). Eventually, each neuron converges to a specific weight, achieving the optimal solution for the neural network. Unsupervised learning includes input but not labels. The network automatically finds potential rules based on input. Semi-supervised learning is between supervised learning and unsupervised learning, including input and a few labels. Reinforcement learning trains the network through interactions with the environment.

ANNs are composed of multiple neurons that are connected by synapses and learn by adjusting the weights of the synapses. Memristors are commonly used to simulate synapses in ANNs. Vector matrix multiplication (VMM) is an important computational module in ANNs, which can be achieved through memristor crossbar array. The resistance of memristor implements multiplication, while Kirchhoff's current law implements addition. Fig. 9 shows a memristor crossbar array. The intersection node of each row and column represents a memristor and G represents conductance. Output vector I can be calculated.

$$\text{Output } I_j = \sum_{i=1}^{3} V_i \times G_{ij} \tag{11}$$

In 2020, Yao et al. constructed a five-layer CNN based on TiN/TaO_x/HfOx/TiN memristors to perform image recognition with accuracy more than 96%. It shows more than two orders of magnitude better power efficiency and one order of magnitude better performance density compared with Tesla V100 GPU [180]. In 2024, Wen et al. constructed a three-layer ANN based on Ti/$NiPS_3$ /Au memristor to perform image recognition with accuracy of 96.4%. Kanghyeok et al. designed a single-layer ANN with $Hf_{0.8}Si_{0.2}O_2$/Al_2O_3/$Hf_{0.5}Si_{0.5}O_2$-based self-rectifying memristors. Because the designed memristor has large selectivity, two-bit operation, low read power and read latency, excellent data retention, the network achieves 100% classification accuracy [181].

4.2 Spiking Neural Networks

Although ANNs have achieved breakthrough progress in many fields, their power consumption and performance are far inferior to those of biological neural networks. There are essential differences between the problem-solving methods of ANNs and biological neurons. Biological neurons communicate through APs, leading to the development of SNNs, where spiking neurons are used as computational units [182]. Since neurons only spike when they reach a threshold, SNNs are sparse computation. Fig. 10 illustrates the differences of neurons between ANNs and SNNs.

Binarized SNNs (BSNNs) are an extreme form of quantized networks, the neuron activations and synaptic weights are represented by binary values [183]. They have many advantages, like high computational efficiency, ultra-low energy consumption, and convenient hardware implementation, but there are also obvious disadvantages, like accuracy loss and difficult training. Digital devices, such as field-programmable gate array (FPGA), have been widely used in BSNNs and have shown good performance [184].

SNNs must consider three aspects: spiking coding, neural circuits, and learning rules. Currently, there are multiple spiking coding schemes available and we mainly discuss three of them. Rate coding encodes spiking frequency [185]; temporal coding encodes timing of individual spikes [186]; phase coding encodes spiking phase relative to reference oscillation [187]. SNNs learning algorithms can be divided into unsupervised learning, such as Bienenstock-Cooper-Munro (BCM) [188], STDP [189] and its modifications [190, 191], SRDP[192]; supervised learning such as backpropagation (BP)-based [193, 194], supervised STDP

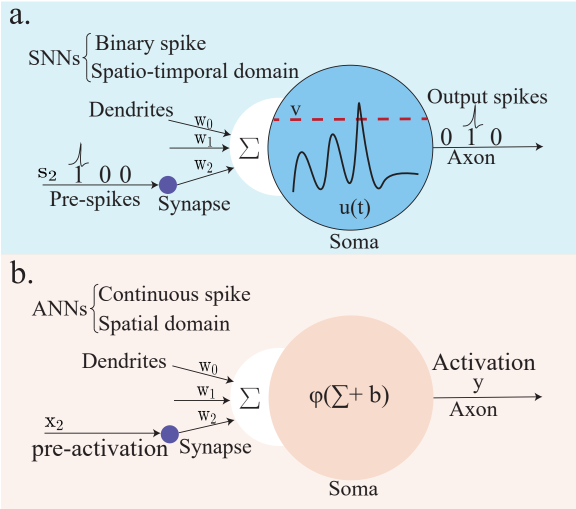

Fig. 10 Comparison of neurons between ANNs and SNNs. (a) The neuron of ANNs; (b) The neuron of SNNs. SNNs=ANNs+Neuronal Dynamics

[195, 196]; reinforcement learning [197, 198]; and conversion from ANNs to SNNs [199, 200]. Below is a brief introduction to some learning rules.

1) BCM: It possesses a sliding synaptic threshold θ_{m} that changes with the activity of postsynaptic neurons. When the postsynaptic spike rates exceeds θ_{m}, the synaptic weight is potentiated; conversely, if it falls below θ_{m}, the weight is depressed.

2) BP: Since the activation function of neurons is non-differentiable, BP cannot train SNNs directly, approximating the derivative with a surrogate gradient is an effective solution.

3) Reward-modulated STDP: It belongs to reinforcement learning. When a neuron makes a correct decision, STDP is applied to reinforce its selectivity. Otherwise, anti-STDP is applied, which encourages the neuron to learn something else.

4) ANNs to SNNs: This approach converts pre-trained ANNs into its equivalent SNNs.

In 2023, Walters et al. constructed a SNN based on graphene-based memristors and neurons with adaptive voltage thresholds, achieving an accuracy of over 80% on the MNIST dataset [201]. In 2024, Yoon et al. proposed a memristor–CMOS hybrid circuit for applying the conventional BP algorithm in SNNs, and it achieves an accuracy of 93.7% on the MNIST-DVS dataset [202]. In 2025, Wang et al. designed a SNN based on TaN/TaO$_x$/TiN memristor and optimized its topological structure, effectively mitigating memristor programming stochasticity. This approach achieves an accuracy of 97.6% on the N-MNIST dataset [203].

Memristive SNNs have lower power consumption and are closer to biological neural networks. But they still face some challenges. At the algorithm level, current training algorithms are not yet mature enough, and there is a need to develop more efficient and hardware specific training algorithms. At the hardware level, the design of memristors is not yet flexible and cannot fully exploit the properties of materials. The instability of the device limits the full memristive SNNs to a small scale. Moreover, high-precision devices need to be further researched.

4.3 Hopfield Neural Network

In 1982, J. J. Hopfield proposed Hopfield neural network (HNN) [204]. It is a brain-like neural network and can exhibit abundant dynamics behaviors due to its special network structure and nonlinear activation function. It has been widely applied in various fields, such as associative memory [205], image encryption [206], optimization problems [207]. The mathematical expression of HNN model can be defined as

$$C_i \dot{x}_i = -\frac{x_i}{R_i} + \sum_{j=1}^{n} w_{ij} f(x_j) + I_i \quad (i, j \in N^*) \tag{12}$$

where C_i, R_i and x_i are the membrane capacitance, membrane resistance and the state variable of the ith neuron, respectively. And w_{ij} represents the synaptic weight value between the ith neuron and the jth neuron. $f(x)$, I_i are the nonlinear activation function and external current of each neuron, respectively.

A generic memristor is defined by

$$\begin{cases} i = W(\varphi)v \\ \dot{\varphi} = f(\varphi, v) \end{cases} \tag{13}$$

where $W(\varphi)$ is the memductance, φ is the memristor state variable, and $f(\varphi, v)$ is the state equation.

According to the different functions of memristors in neural networks, memristive HNN can be classified into four categories.

1) Memristor-autapse-based HNN

This can be constructed by replacing resistive self-connection synaptic weights with memristive self-connection synaptic weights.

Over the past years, many different HNNs with memristor autapses have been constructed, and various dynamics behaviors have been revealed. Hidden dynamics behaviors have been discovered in single neuron HNN using hyperbolic memristors autapse [208]. Ref. [209] constructed a fraction-order HNN with four neurons using LAMs with multistability as autapse. The system experiences the transition between period and chaos, and there are infinite coexisting attractors. Ref. [210] constructed a two-memristor-based HNN by replacing the resistive self-connection synaptic weights of two neurons with memristor and offset-control plane coexisting attractors are found.

2) Memristor-synapse-based HNN

The model can be constructed by replacing resistive coupling synaptic weights with memristive coupling synaptic weights.

At present, there are extensive related studies. Ref. [211] constructed a three-neuron HNN with a tristable LAM synapse. The equilibrium points of the system depend on the coupling weight of the memristor synapse. Coexistence of multiple stable modes and bursting oscillations are also found. Any multi-scroll hyperchaotic attractor was found in four-neuron HNN with self-connection and coupled-connection using multi-segment function memristors [212]. Ref. [213] used LAMs as synapses to connect two identical/disparate HNNs. Identical HNNs exhibit synchronous transitions, but disparate HNNs exhibit complex and rich dynamics, including hyperchaos, chaos, quasi-period, and multi-stable patterns.

3) HNN under external electromagnetic radiation

As mentioned earlier, flux-controlled memristors can simulate electromagnetic induction current. Electromagnetic induction current I_M can be defined by

$$I_M = \rho W(\varphi) x_i \tag{14}$$

where ρ represents the coupling strength between membrane potential and magnetic flux. x_i is the membrane potential of the neuron under electromagnetic radiation.

Ref. [214] discussed the hidden dynamics of three-neuron HNN, such as hyperchaos, transient hyperchaos. Ref. [215] proposed a new memristor model with controllable number of power interruption steady states to simulate electromagnetic radiation in HNN. A series of complex chaotic phenomena are found, including memristor-controlled multi-scroll attractors, symmetric bifurcation behaviors, initial offset boosting coexistence. Ref. [216] considered the effects of single and dual electromagnetic radiation using memristors on a four-neuron HNN. With the memristors increasing, rich chaotic dynamics such as period, chaos, transient chaos, quasi-period, and multi-period are observed.

4) HNN under internal electromagnetic field

When possessing a potential difference between two neurons, an internal electromagnetic induction current appears in the neural network, which can be described by a flux-controlled memristor synapse. Electromagnetic induction current I_M can be defined by

$$I_M = \rho W(\varphi)(x_i - x_j) \tag{15}$$

where ρ represents coupling strength between memristor and neuron, $(x_i - x_j)$ represents potential difference between two neurons.

Ref. [217] presented a third-order non-ideal memristor synapse-coupled two-neuron HNN and it behaves bi-stability of coexisting chaotic and stable point attractors. Ref. [218] investigated HNN with different numbers of internal electromagnetic induction currents with hyperbolic-type memristors. This system behaved coexisting bifurcation behaviors, periodic and chaotic bubbles, riddled basins of attraction. Ref. [219] proposed a two-neuron HNN using a piecewise linear function memristor and this system behaves multistability of coexisting chaos, periodic limit cycles, and stable point attractors.

Neural network dynamics analysis provides theoretical references for the construction and application of adaptive, low-power, and high-computational-capacity biomimetic neural networks. Although neural networks implemented with different memristors as synapses can mimic some characteristics of biological neural networks, they lack theoretical guidance from biological neural systems and are unable to fully represent the energy transfer relationships and synaptic plasticity of biological neural systems. In the future, guided by the latest neurobiological theories, it will become an inevitable trend to construct more biomimetic neural networks, synapses, and neuron models and conduct dynamics research.

4.4 Application

4.4.1 Physiological Signal Processing

Physiological signals provide rich cognitive and health-related information, which is beneficial for medical diagnosis and disease monitoring. They include electroencephalogram (EEG), electrocardiogram (ECG), electromyogram (EMG) and electrooculogram (EOG), etc. In 2023, Yang et al. proposed a SNNs based on VO_2 memristors, which can analyze physiological signals encoded in spikes. It achieved accuracies of 95.83% and 99.79% in arrhythmia classification and epileptic seizure detection, respectively [220]. In 2024, Bak et al. utilized memristive CNN to classify stress states, and demonstrated that its performance was superior to that of existing CNN models [221]. In 2025, Li et al. designed a VO_2-based adaptive LIF model and constructed a SNN for EMG recognition, achieving a classification accuracy of 97.1% [222].

4.4.2 Edge Intelligence Device

Edge computing has high requirements for power consumption, latency, and area. Memristor-based neural networks are a promising approach to realize edge intelligence devices. In 2022, Wu et al. constructed a SNN for speech recognition based on $W/MgO/SiO_2/Mo$ memristors, achieving a high speech recognition accuracy of 94% [223]. In 2025, Zhang et al. proposed a self-rectifying memristor based on the $TiN/HfO_x/Pt$ structure for neural networks, achieving high-accuracy real-time classification for autonomous driving [224]. Chen et al. proposed a HfO_x-based memristive SNN circuit for goal-oriented navigation, enabling the agent to exhibit capabilities of random exploration, cognitive map construction, obstacle avoidance, and navigation. This circuit primarily consists of three core modules: the place cell module encodes and real-time represents the agent's spatial position; the action cell module determines the subsequent movement direction; and the learning module provides a bio-inspired learning approach adaptive to delayed and sparse rewards [225].

5 Conclusion

This review discusses the realization of synapses, neurons, and neural networks using memory devices. Finally, four research directions are proposed for future neuromorphic networks based on memory devices. 1) Fabricate more biomimetic memristors. Although current memristor devices can simulate neurons or synapses, they lack sufficient biomimetic properties and numerical feasibility, necessitating further clarification of the memristor mechanism. 2) Building highly reliable simulation frameworks. This enables low-cost and rapid research on algorithms and scalability of SNNs, while providing guidance for hardware implementation. 3) Develop larger neural networks. Although numerous neural network models are available, most are limited to relatively small scales. As AI technology advances, neural network models with larger numbers of neurons and more complex architectures will become increasingly essential. 4) Spiking coding for SNNs. The study of spike coding is essential for advancing SNNs, as it plays a fundamental role in how information is represented and processed. Coding technique not only influences the computational efficiency of SNNs but also impacts their performance in practical applications. As such, optimizing the coding method is critically important.

Declarations

Funding. This work is supported by the National Natural Science Foundation of China (62171182), Natural Science Foundation Project of Hunan, China (2025JJ50345), Natural Science Foundation Project of Chongqing, Chongqing Science and Technology Commission (CSTB2022NSCQ-MSX0770).

Author contributions. Jingru Sun and Jingwen Sun wrote the main manuscript text, Xiaosong Li prepared the content of the Synapses and Neurons Model, and Qinghui Hong and Chunhua Wang prepared the content of the Neural Networks. Yichuang Sun provided guidance and inspection

for the entire paper. All authors reviewed the manuscript.

Data availability. Data sharing is not applicable to this article, as no datasets were generated or analyzed during the current study.

Conflict of interest. The authors declare that they have no conflict of interest.

References

[1] Yu, S.: Neuro-inspired computing with emerging nonvolatile memorys. Proceedings of the IEEE **106**(2), 260–285 (2018)

[2] Shankar, S., Reuther, A.: Trends in energy estimates for computing in AI/Machine learning accelerators, supercomputers, and compute-intensive applications. 2022 IEEE High Performance Extreme Computing Conference (HPEC), Waltham, MA, USA, 2022 (2022)

[3] Furber, S.: Large-scale neuromorphic computing systems. Journal of Neural Engineering **13**(5), 051001 (2016)

[4] Balasubramanian, V.: Heterogeneity and efficiency in the brain. Proceedings of the IEEE **103**(8), 1346–1358 (2015)

[5] Herculano-Houzel, S.: The human brain in numbers: a linearly scaled-up primate brain. Frontiers in Human Neuroscience **3**, 31 (2009)

[6] Bullmore, E.T., Sporns, O.: The economy of brain network organization. Nature Reviews Neuroscience **13**(5), 336–349 (2012)

[7] Fries, P.: A mechanism for cognitive dynamics: neuronal communication through neuronal coherence. Trends in Cognitive Sciences **9**(10), 474–480 (2005)

[8] Amit, D.J., Mongillo, G.: Spike-driven synaptic dynamics generating working memory states. Neural Computation **15**(3), 565–596 (2003)

[9] Wang, X.: Decision making in recurrent neuronal circuits. Neuron **60**(2), 215–234 (2008)

[10] Sun, J., Ma, W., Xiaosong Li, Y.S., Hong, Q., Zhang, J.: Design and application of algae light sensing circuit based on memristor. Nonlinear Dynamics **113**(11), 13747–13770 (2025)

[11] Merolla, P.A., Arthur, J.V., Alvarez-Icaza, R., *et al.*: A million spiking-neuron integrated circuit with a scalable communication network and interface. Science **345**(6197), 668–673 (2014)

[12] Davies, M., Srinivasa, N., Lin, T.-H., *et al.*: Loihi: a neuromorphic manycore processor with on-chip learning. IEEE Micro **38**(1), 82–99 (2018)

[13] Burns, M.E., Augustine, G.J.: Synaptic structure and function: dynamic organization yields architectural precision. Cell **83**(2), 187–194 (1995)

[14] Fonnum, F.: Glutamate: a neurotransmitter in mammalian brain. Journal of Neurochemistry **42**(1), 1–11 (1984)

[15] Bowery, N.G., Smart, T.G.: GABA and glycine as neurotransmitters: a brief history. British Journal of Pharmacology **147**, 109–119 (2006)

[16] Bliss, T.V.P., Lømo, T.: Long-lasting potentiation of synaptic transmission in the dentate area of the anaesthetized rabbit following stimulation of the perforant path. The Journal of Physiology **232**(2), 31–356 (1973)

[17] Neves, G., Cooke, S.F., Bliss, T.V.P.: Synaptic plasticity, memory and the hippocampus: a neural network approach to causality. Nature reviews. Neuroscience **9**, 65–75 (2008)

[18] Takeuchi, T., Duszkiewicz, A.J., Morris, R.G.M.: The synaptic plasticity and memory hypothesis: encoding, storage and persistence. Phil. Trans. R. Soc. B **369**(1633), 20130288 (2014)

[19] Debanne, D., Guérineau, N.C., Gähwiler, B.H., Thompson, S.M.: Paired-pulse facilitation and depression at unitary synapses in rat hippocampus: quantal fluctuation affects subsequent release. The Journal of Physiology **1**, 163–176 (1996)

[20] Citri, A., Malenka, R.C.: Synaptic plasticity: multiple forms, functions, and mechanisms. Neuropsychopharmacology **33**(1), 18–41 (2007)

[21] Abbott, L.F., Nelson, S.B.: Synaptic plasticity: taming the beast. Nature Neuroscience **3**, 1178–1183 (2000)

[22] Song, S., Miller, K.D., Abbott, L.F.: Competitive hebbian learning through spike-timing-dependent synaptic plasticity. Nature Neuroscience **3**(9), 919–926 (2000)

[23] Pfister, J.P., Gerstner, W.: Triplets of spikes in a model of spike timing-dependent plasticity. The Journal of Neuroscience **26**(38), 9673–9682 (2006)

[24] Lammie, C., Hamilton, T.J., Schaik, A., Azghadi, M.R.: Efficient FPGA implementations of pair and triplet-based STDP for neuromorphic architectures. IEEE Transactions on Circuits and Systems I: Regular Papers **66**(4), 1558–1570 (2019)

[25] Yang, S., Wang, H., Pang, Y., *et al.*: Integrating visual perception with decision making in neuromorphic fault-tolerant quadruplet-spike learning framework. IEEE Transactions on Systems, Man, and Cybernetics: Systems **54**(3), 1502–1514 (2024)

[26] C.Magee, J., Grienberger, C.: Synaptic plasticity forms and functions. Physiological reviews **86**(3), 1033–1048 (2006)

[27] Fernandes, D., Carvalho, A.L.: Mechanisms of homeostatic plasticity in the excitatory synapse. Journal of Neurochemistry **139**(6), 973–996 (2016)

[28] Yang, X., Brady, T., Wu, A., *et al.*: Research progress on memristor: from synapses to computing systems. IEEE Transactions on Circuits and Systems I: Regular Papers **69**(5), 1845–1857 (2022)

[29] Jeong, H., Shi, L.: Memristor devices for neural networks. Journal of Physics D: Applied Physics **52**(2), 1 (2019)

[30] Chua, L.O.: Memristor - the missing circuit element. IEEE Transactions on Circuit Theory **18**(5), 507–519 (1971)

[31] Chua, L.O., Kang, S.M.: Memristive devices and systems. Proceedings of the IEEE **64**(2), 209–223 (1976)

[32] Strukov, D.B., Snider, G.S., Stewart, D.R., Williams, R.S.: The missing memristor found. Nature **453**, 80–83 (2008)

[33] Itoh, M., Chua, L.O.: Memristor oscillators. International Journal of Bifurcation and Chaos **18**(11), 3183–3206 (2008)

[34] Wang, X., Chen, Y., Xi, H., *et al.*: Spintronic memristor through spin-torque-induced magnetization motion. IEEE Electron Device Letters **30**(3), 294–297 (2009)

[35] Chen, Y., Wang, X.: Compact modeling and corner analysis of spintronic memristor. 2009 IEEE/ACM International Symposium on Nanoscale Architectures, San Francisco, CA, USA, 2009 (2009)

[36] Kvatinsky, S., Friedman, E.G., Kolodny, A., Weiser, U.C.: TEAM: threshold adaptive memristor model. IEEE Transactions on Circuits and Systems I: Regular Papers **60**(1), 211–221 (2013)

[37] Kvatinsky, S., Ramadan, M., Friedman, E.G., Kolodny, A.: VTEAM: a general model for voltage-controlled memristors. IEEE Transactions on Circuits and Systems II: Express Briefs **62**(8), 786–790 (2015)

[38] Pickett, M.D., Strukov, D.B., Borghetti, J.L., *et al.*: Switching dynamics in titanium dioxide memristive devices. Journal of Applied Physics **106**(7), 074508–0745086 (2009)

[39] Chua, L.O.: If it's pinched it's a memristor.

Semiconductor Science Technology **29**(10), 104001 (2014)

[40] Chua, L.O.: Local activity is the origin of complexity. International Journal of Bifurcation and Chaos in Applied Sciences and Engineering **15**(11), 3435–3456 (2005)

[41] Chua, L.O.: Memristor, hodgkin–huxley, and edge of chaos. Nanotechnology **24**(38), 383001 (2013)

[42] Sah, M.P., Kim, H., Chua, L.O.: Brains are made of memristors. IEEE Circuits and Systems Magazine **14**(1), 12–36 (2014)

[43] Wang, Z., Joshi, S., Savel'ev, S.E., *et al.*: Memristors with diffusive dynamics as synaptic emulators for neuromorphic computing. Nature Materials **16**(1), 101–108 (2016)

[44] Yin, J., Zeng, F., Wan, Q., *et al.*: Adaptive crystallite kinetics in homogenous bilayer oxide memristor for emulating diverse synaptic plasticity. Advanced Functional Materials **28**(19), 1 (2018)

[45] Sahu, M.C., Jena, A.K., Mallik, S.K., *et al.*: Reconfigurable low-power TiO_2 memristor for integration of artificial synapse and nociceptor. ACS Applied Materials and Interfaces **15**(21), 25713–25725 (2023)

[46] Xiao, Z., Huang, J.: Energy-efficient hybrid perovskite memristors and synaptic devices. Advanced Electronic Materials **2**, 1600100 (2016)

[47] Gong, Y., Wang, Y., Li, R., *et al.*: Tailoring synaptic plasticity in perovskite QD-based asymmetric memristor. Journal of Materials Chemistry C **8**(9), 2985–2992 (2020)

[48] Kim, S.J., Lee, T.H., Yang, J.-M., *et al.*: Vertically aligned two-dimensional halide perovskites for reliably operable artificial synapses. Materials Today **52**, 19–30 (2022)

[49] Kuzum, D., Jeyasingh, R.G.D., Lee, B., Wong, H.S.P.: Nanoelectronic programmable synapses based on phase change materials for brain-inspired computing. Nano Letters **12**(5), 2179–2186 (2012)

[50] Yan, X., Zhao, Q., Chen, A.P., *et al.*: Vacancy-induced synaptic behavior in 2 D WS_2 nanosheet-based memristor for low-power neuromorphic computing. Small **15**(24), 1901423 (2019)

[51] Yu, T., Zhao, Z., Jiang, H., *et al.*: $MoTe_2$-based low energy consumption artificial synapse for neuromorphic behavior and decimal arithmetic. Materials Today Chemistry **27**, 101268 (2023)

[52] Zhang, C., Tai, Y.-T., Shang, J., *et al.*: Synaptic plasticity and learning behaviours in flexible artificial synapse based on polymer/viologen system. Journal of Materials Chemistry C **4**(15), 3217–3223 (2016)

[53] Mao, J., Zhou, L., Ren, Y., *et al.*: A bio-inspired electronic synapse using solution processable organic small molecule. Journal of Materials Chemistry C **7**(6), 1491–1501 (2019)

[54] Yan, X., Li, X., Zhou, Z., *et al.*: Flexible transparent organic artificial synapse based on the tungsten/egg albumen/indium tin oxide/polyethylene terephthalate memristor. ACS Applied Materials and Interfaces **11**(20), 18654–18661 (2019)

[55] Yi, W., Tsang, K.K., Lam, S.K., *et al.*: Biological plausibility and stochasticity in scalable VO_2 active memristor neurons. Nature Communications **9**(1), 1–10 (2018)

[56] Jiang, B., Ke, S., Tao, Z., *et al.*: In-depth analysis of core-shell filaments in nonvolatile NbO_x memristive device as an artificial synapse for multifunctional bionic applications. Science China Technological Sciences **66**(12), 3596–3603 (2023)

[57] Mannan, Z.I., Choi, H., Kim, H.: Chua corsage memristor oscillator via hopf bifurcation. International Journal of Bifurcation and Chaos in Applied Sciences and Engineering **26**(4), 1630009 (2016)

[58] Li, Z., Zhou, H., Wang, M., *et al.*: Coexisting firing patterns and phase synchronization in locally active memristor coupled neurons with HR and FN models. Nonlinear Dynamics **104**(2), 1455–1473 (2021)

[59] Lai, Q., Yang, L.: Discrete memristor applied to construct neural networks with homogeneous and heterogeneous coexisting attractors. Chaos, Solitons and Fractals **174**, 113807 (2023)

[60] Chen, M., Zhang, Y., Zhang, Y., *et al.*: Transition and bifurcation mechanism of firing activities in memristor synapse-coupled Hindmarsh–Rose bi-neuron model. Chaos, Solitons and Fractals **188**, 115574 (2024)

[61] Hu, J., Bao, H., Xu, Q., *et al.*: Synchronization generations and transitions in two map-based neurons coupled with locally active memristor. Chaos, Solitons and Fractals **184**, 114993 (2024)

[62] Ling, H., Koutsouras, D.A., Kazemzadeh, S., *et al.*: Electrolyte-gated transistors for synaptic electronics, neuromorphic computing, and adaptable biointerfacing. Applied Physics Reviews **17**(1), 1–22 (2020)

[63] Zhang, F., Li, C., Li, Z., *et al.*: Recent progress in three-terminal artificial synapses based on 2D materials: from mechanisms to applications. Microsystems and Nanoengineering **9**(1), 1–17 (2023)

[64] Van Tho, L., Baeg, K.J., Noh, Y.Y.: Organic nano-floating-gate transistor memory with metal nanoparticles. Nano Convergence **3**(1), 10 (2016)

[65] Paul, T., Ahmed, T., Tiwari, K.K., *et al.*: A high-performance MoS_2 synaptic device with floating gate engineering for neuromorphic computing. 2D Materials **6**(4), 045008 (2019)

[66] Cho, H., Lee, D., Ko, K., *et al.*: Double-floating-gate van der Waals transistor for high-precision synaptic operations. ACS Nano **17**, 7384–7393 (2023)

[67] Zhu, J., Wang, Z., Liu, D., *et al.*: Flexible low-voltage MXene floating-gate synaptic transistor for neuromorphic computing and cognitive learning. Advanced Functional Materials **34**(40), 1 (2024)

[68] Yang, J.T., Ge, C., Du, J.Y., *et al.*: Artificial synapses emulated by an electrolyte-gated tungsten-oxide transistor. Advanced Materials **30**(34), 1801548 (2018)

[69] Liu, G., Li, Q., Shi, W., *et al.*: Ultralow-power and multisensory artificial synapse based on electrolyte-gated vertical organic transistors. Advanced Functional Materials **32**(27), 1 (2022)

[70] Zhu, L., Lin, J., Zhu, Y., *et al.*: Flexible organic electrochemical transistors for energy-efficient neuromorphic computing. Nanomaterials **14**(14), 1195 (2024)

[71] Jerry, M., Chen, P.-Y., Zhang, J., et al.: Ferroelectric FET analog synapse for acceleration of deep neural network training. 2017 IEEE International Electron Devices Meeting (IEDM), San Francisco, CA, USA, 2017 (2017)

[72] Xia, F., Xia, T., Xiang, L., *et al.*: Carbon nanotube-based flexible ferroelectric synaptic transistors for neuromorphic computing. ACS Applied Materials and Interfaces **14**(26), 30124–30132 (2022)

[73] Song, C., Kim, D., Lee, S., Kwon, H.: Ferroelectric 2D SnS_2 analog synaptic FET. Advanced Science **11**(16), 2308588 (2024)

[74] Wu, Q., Wang, J., Cao, J., *et al.*: Photoelectric plasticity in oxide thin film transistors with tunable synaptic functions. Advanced Electronic Materials **4**(12), 1–8 (2018)

[75] Xin, Z., Tan, Y., Chen, T., *et al.*: Visible-light-stimulated synaptic InGaZnO phototransistors enabled by wavelength-tunable perovskite quantum dots. Nanoscale Advances **3**(17), 5046–5052 (2021)

[76] Chen, Y., Wang, Z., Du, J., *et al.*: Wrinkled rhenium disulfide for anisotropic nonvolatile

memory and multiple artificial neuromorphic synapses. ACS Nano **18**, 30871–30883 (2024)

[77] Stadelmann, C., Timmler, S., Barrantes-Freer, A., Simons, M.: Myelin in the central nervous system: structure, function, and pathology. Physiological Reviews **99**(3), 1381–1431 (2019)

[78] Palay, S.L., Sotelo, C., Peters, A., Orkand, P.M.: The axon hillock and the initial segment. The Journal of Cell Biology **38**(1), 193–201 (1968)

[79] Benes, F.M., Turtle, M., Khan, Y., Farol, P.: Myelination of a key relay zone in the hippocampal formation occurs in the human brain during childhood, adolescence, and adulthood. Archives of General Psychiatry **51**(6), 477–484 (1994)

[80] Abbott, L.F.: Lapicque's introduction of the integrate-and-fire model neuron (1907). Brain Research Bulletin **50**(5), 303–304 (1999)

[81] Brunel, N., Rossum, M.C.W.V.: Lapicque's 1907 paper: from frogs to integrate-and-fire. Biological Cybernetics **97**(5), 337–339 (2007)

[82] Hodgkin, A.L., Huxley, A.F.: A quantitative description of membrane current and its application to conduction and excitation in nerve. The Journal of Physiology **4**, 500–544 (1952)

[83] Kopell, G.B.E.: Parabolic bursting in an excitable system coupled with a slow oscillation. Siam Journal on Applied Mathematics **46**(2), 233–253 (1986)

[84] Ermentrout, B.: Type I membranes, phase resetting curves, and synchrony. Neural Computation **8**(5), 979–1001 (1996)

[85] Latham, P.E., Richmond, B.J., Nelson, P.G., Nirenberg, S.: Intrinsic dynamics in neuronal networks. I. theory. Journal of Neurophysiology **83**(2), 808–827 (2000)

[86] Smith, G.D., Cox, C.L., Sherman, S.M., Rinzel, J.: Fourier analysis of sinusoidally driven thalamocortical relay neurons and a minimal integrate-and-fire-or-burst model. Journal of Neurophysiology **83**(1), 588–610 (2000)

[87] Izhikevich, E.M.: Resonate-and-fire neurons. Neural Networks **14**(6-7), 883 (2001)

[88] FourcaudTrocmé, N., Hansel, D., Vreeswijk, C.V., Brunel, N.: How spike generation mechanisms determine the neuronal response to fluctuating inputs. Journal of Neuroscience **23**(37), 11628 (2003)

[89] Jolivet, R., Lewis, T.J., Gerstner, W.: The spike response model: a framework to predict neuronal spike trains. Lecture Notes in Computer Science **2714**(1), 173 (2003)

[90] Brette, R.: Adaptive exponential integrate-and-fire model as an effective description of neuronal activity. Journal of Neurophysiology **94**(5), 3637 (2005)

[91] Fitzhugh, R.: Impulses and physiological states in theoretical models of nerve membrane. Biophysical Journal **1**(6), 445–466 (1961)

[92] Nagumo, J.S., Arimoto, S., Yoshizawa, S.: An active pulse transmission line simulating nerve axon. Proceedings of the Ire **50**(10), 2061–2070 (1962)

[93] Connor, J.A., Stevens, C.F.: Prediction of repetitive firing behaviour from voltage clamp data on an isolated neurone soma. The Journal of Physiology **213**(1), 31–53 (1971)

[94] Connor, J.A., Walter, D., Mckown, R.: Neural repetitive firing: modifications of the hodgkin-huxley axon suggested by experimental results from crustacean axons. Biophysical Journal **18**(1), 81–102 (1977)

[95] Morris, C., Lecar, H.: Voltage oscillations in the barnacle giant muscle fiber. Biophysical Journal **35**(1), 193–213 (1981)

[96] Hindmarsh, J.L., Rose, R.M.: A model of the

nerve impulse using two first-order differential equations. Nature **296**(5853), 162–164 (1982)

[97] Hindmarsh, J.L., Rose, R.M.: A model of neuronal bursting using three coupled first order differential equations. Proc. R. Soc. Lond. B **221**(1222), 87–102 (1984)

[98] Rose, R.M., Hindmarsh, J.L.: A model of a thalamic neuron. Proc. R. Soc. Lond. B **225**(1239), 161–193 (1985)

[99] Rose, R.M., Hindmarsh, J.L.: The assembly of ionic currents in a thalamic neuron I. The three-dimensional model. Proc. R. Soc. Lond. B **237**(1288), 267–288 (1989)

[100] Chay, T.R.: Chaos in a three-variable model of an excitable cell. Physica D **16**, 233–242 (1985)

[101] Wilson, H.R.: Simplified dynamics of human and mammalian neocortical neurons. Journal of Theoretical Biology **200**(4), 375–388 (1999)

[102] Izhikevich, E.M.: Simple model of spiking neurons. IEEE Transactions on Neural Networks **14**(6), 1569–72 (2003)

[103] Wang, R., Tsuda, I., Zhang, Z.: A new work mechanism on neuronal activity. International Journal of Neural Systems **25**(3), 1450037 (2015)

[104] Wang, R., Wang, Z., Zhu, Z.: The essence of neuronal activity from the consistency of two different neuron models. Nonlinear Dynamics **92**(3), 973–982 (2018)

[105] Li, X., Sun, J., Sun, Y., *et al.*: A power-adaptive neuron model and circuit implementation. Nonlinear Dynamics **113**(4), 3763–3780 (2025)

[106] Fukai, T., Tanaka, S.: A simple neural network exhibiting selective activation of neuronal ensembles: from winner-take-all to winners-share-all. Neural Computation **9**(1), 77 (1997)

[107] Mcculloch, W.S., Pitts, W.: A logical calculus of the ideas immanent in nervous activity. Bulletin of Mathematical Biophysics **5**, 115–133 (1943)

[108] Wilson, H.R., Cowan, J.D.: A mathematical theory of the functional dynamics of cortical and thalamic nervous tissue. Kybernetik **13**(2), 55 (1973)

[109] Stiefel, K.M., Ermentrout, G.B.: Neurons as oscillators. Journal of Neurophysiology **116**(6), 2950–2960 (2016)

[110] Zhang, Y., Xu, Y., Yao, Z., Ma, J.: A feasible neuron for estimating the magnetic field effect. Nonlinear Dynamics **102**(3), 1849–1867 (2020)

[111] Shi, F., Cao, Y., Banerjee, S., Mou, J.: A neuronal circuit based on a second-order memristor. Nonlinear Dynamics **113**(10), 12165–12183 (2025)

[112] Ma, J., Guo, Y.: Model approach of electromechanical arm interacted with neural circuit, a minireview. Chaos, Solitons and Fractals **183**, 114925 (2024)

[113] Shao, Y., Wu, F., Wang, Q.: Excitability and synchronization of vanadium dioxide memristor-inspired neurons. Mathematics and Computers in Simulation **233**, 99–116 (2025)

[114] Chen, B., Liu, Y., Bao, H., *et al.*: Coexisting and bursting oscillations in a second-order RC-oscillator-based piecewise linear neuron circuit. Nonlinear Dynamics **113**, 17141–17159 (2025)

[115] Cazelles, B., Courbage, M., Rabinovich, M.I.: Anti-phase regularization of coupled chaotic maps modelling bursting neurons. American Institute of Physics **56**(4), 504–509 (2003)

[116] Rulkov, N.F.: Regularization of synchronized chaotic bursts. Physical Review Letters **86**(1), 183–6 (2001)

[117] Chialvo, D.R.: Generic excitable dynamics on a two-dimensional map. Chaos, Solitons

and Fractals **5**(3), 461–479 (1995)

[118] Zandi-Mehran, N., Panahi, S., Hosseini, Z., *et al.*: One dimensional map-based neuron model: A phase space interpretation. Chaos, Solitons and Fractals **132**, 109558 (2020)

[119] Yang, Y., Zhang, X., Chen, P., *et al.*: Memristive Hodgkin–Huxley neurons with diverse firing patterns for high-order neuromorphic computing. Advanced Intelligent Systems **7**(2), 2400383 (2025)

[120] Li, X., Sun, J., Sun, Y., *et al.*: Design of artificial neurons of memristive neuromorphic networks based on biological neural dynamics and structures. IEEE Transactions on Circuits and Systems I: Regular Papers **71**(5), 1–14 (2024)

[121] M.Izhikevich, E.: Which model to use for cortical spiking neurons? IEEE Transactions on Neural Networks **15**(5), 1063–1070 (2004)

[122] BERG, T.O., SAND, O.: Spontaneous all-or-nothing action potentials in the ciliate bursaridium difficile. Journal of Eukaryotic Microbiology **41**(1), 13–17 (1994)

[123] Guido, W., Lu, S.M., Sherman, S.M.: Relative contributions of burst and tonic responses to the receptive field properties of lateral geniculate neurons in the cat. Journal of Neurophysiology **68**(6), 2199–2211 (1992)

[124] Kim, U., McCormick, D.A.: The functional influence of burst and tonic firing mode on synaptic interactions in the thalamus. The Journal of Neuroscience **18**(22), 9500–9516 (1998)

[125] Stecker, G.C., Middlebrooks, J.C.: Distributed coding of sound locations in the auditory cortex. Biological Cybernetics **89**(5), 341–349 (2003)

[126] Gollisch, T., Meister, M.: Rapid neural coding in the retina with relative spike latencies. Science **319**(5866), 1108–1111 (2008)

[127] Ha, G.E., Cheong, E.: Spike frequency adaptation in neurons of the central nervous system. Experimental Neurobiology **26**(4), 179–185 (2017)

[128] Benda, J., Longtin, A., Maler, L.: Spike-frequency adaptation separates transient communication signals from background oscillations. Journal of Neuroscience **25**(9), 2312–2321 (2005)

[129] Zhao, Z., Huaguang, G.: Transitions between classes of neuronal excitability and bifurcations induced by autapse. Scientific Reports **7**, 6760 (2017)

[130] Lampl, I., Yarom, Y.: Subthreshold oscillations of the membrane potential: a functional synchronizing and timing device. Journal of Neurophysiology **70**(5), 2181–2186 (1993)

[131] Torrealdea, F.J., Sarasola, C., d'Anjou, A., *et al.*: Energy efficiency of information transmission by electrically coupled neurons. BioSystems **97**(1), 60–71 (2009)

[132] Sarasola, C., Torrealdea, F.J., d'Anjou, A., *et al.*: Energy balance in feedback synchronization of chaotic systems. Physical Review. E, Statistical, Nonlinear, and Soft Matter Physics **69**(1), 011606 (2004)

[133] Ma, J.: Biological neurons to neural circuit, review from physical perspective. Nonlinear Dynamics (2025)

[134] Ma, J., Wu, F., Jin, W., *et al.*: Calculation of Hamilton energy and control of dynamical systems with different types of attractors. Chaos **27**(5), 053108 (2017)

[135] Liu, B., Peng, X., Li, C.: Firing behaviors of memristor-based Rulkov neuron map using energy method. AEU: International Journal of Electronics and Communications **178**, 155283 (2024)

[136] Shi, F., Cao, Y., Banerjee, S., Mou, J.: Firing behaviors of memristor-based Rulkov neuron map using energy method. Nonlinear Dynamics **113**(10), 12165–12183 (2025)

[137] Yang, F., Xu, Y., Ma, J.: A memristive neuron and its adaptability to external electric

field. Chaos **33**(2), 023110 (2023)

[138] Torrealdea, F.J., d'Anjou, A., Graña, M., Sarasola, C.: Energy aspects of the synchronization of model neurons. Physical Review. E, Statistical, Nonlinear, and Soft Matter Physics **74**(1), 011905 (2006)

[139] Song, X., Jin, W., Ma, J.: Energy dependence on the electric activities of a neuron. Chinese Physics B **24**(12), 128710 (2015)

[140] Yang, Y., Ma, J., Xu, Y., Jia, Y.: Energy dependence on discharge mode of Izhikevich neuron driven by external stimulus under electromagnetic induction. Cognitive Neurodynamics **15**(2), 265–277 (2021)

[141] Usha, K., Subha, P.A.: Energy feedback and synchronous dynamics of Hindmarsh-Rose neuron model with memristor. Chinese Physics B **28**(2), 137–146 (2019)

[142] Yao, Z., Zhou, P., Zhu, Z., Ma, J.: Phase synchronization between a light-dependent neuron and a thermosensitive neuron. Neurocomputing **423**, 518–534 (2021)

[143] Lu, Y., Li, H., Li, C.: Electrical activity and synchronization of memristor synapse-coupled HR network based on energy method. Neurocomputing **544**, 126246 (2023)

[144] Xie, Y., Ye, Z., Li, X., *et al.*: A novel memristive neuron model and its energy characteristics. Cognitive Neurodynamics **18**(4), 1989–2001 (2024)

[145] Lv, M., Wang, C., Ren, G., *et al.*: Model of electrical activity in a neuron under magnetic flow effect. Nonlinear Dynamics **85**(3), 1479–1490 (2016)

[146] Wu, F., Wang, C., Xu, Y., Ma, J.: Model of electrical activity in cardiac tissue under electromagnetic induction. Scientific Reports **6**(1), 28 (2016)

[147] Wang, Y., Gong, Y., Huang, S., *et al.*: Memristor-based biomimetic compound eye for real-time collision detection. Nature Communications **12**(1), 5979 (2021)

[148] Shan, X., Liu, Z., Tao, Y., *et al.*: Light-controlled threshold switching memristive neuron devices for color photoreceptor. IEEE Electron Device Letters **45**(10), 1815–1818 (2024)

[149] Xu, Y., Gao, S., Li, Z., *et al.*: Adaptive Hodgkin–Huxley neuron for retina-inspired perception. Advanced Intelligent Systems **4**(12), 2200210 (2022)

[150] Yan, X., Jia, X., Zhang, Y., *et al.*: A low-power Si:HfO_2 ferroelectric tunnel memristor for spiking neural networks. Nano Energy **107**, 108091 (2023)

[151] Guo, Y., Song, X., Ma, J.: Control electromechanical arms by using a neural circuit. Nonlinear Dynamics **113**(2), 1605–1622 (2025)

[152] Guo, Y., Ma, J.: An electromechanical arm model controlled by artificial muscles. Science China Technological Sciences **68**, 1420403 (2025)

[153] Pickett, M.D., Medeiros-Ribeiro, G., Williams, R.S.: A scalable neuristor built with Mott memristors. Nature Materials **12**(2), 114–117 (2012)

[154] Li, X., Sun, J., Ma, W., *et al.*: Adaptive biomimetic neuronal circuit system based on myelin sheath function. IEEE Transactions on Consumer Electronics **70**(1), 3669–3679 (2024)

[155] Li, X., Sun, J., Sun, Y., Zhang, J.: Synaptic and myelin plasticity and their synergistic effects in neuromorphic networks. IEEE Transactions on Circuits and Systems I: Regular Papers, 1–14 (2025)

[156] Chen, M., Qi, J., Xu, Q., Bao, B.: Quasi-period, periodic bursting and bifurcations in memristor-based FitzHugh-Nagumo circuit. AEU: International Journal of Electronics and Communications **110**, 152840 (2019)

[157] Wang, Y., Min, F., Cheng, Y., Dou, Y.: Dynamical analysis in dual-memristor-based FitzHugh–Nagumo circuit and its coupling finite-time synchronization. The European Physical Journal Special Topics **230**(7), 1751–1762 (2021)

[158] Chen, X., Wang, N., Wang, Y., *et al.*: Memristor initial-offset boosting and its bifurcation mechanism in a memristive FitzHugh-Nagumo neuron model with hidden dynamics. Chaos, Solitons and Fractals **174**, 113836 (2023)

[159] Bao, H., Zhu, D., Liu, W., *et al.*: Memristor synapse-based Morris–Lecar model: Bifurcation analyses and FPGA-based validations for periodic and chaotic bursting/spiking firings. International Journal of Bifurcation and Chaos **30**(3), 2050045 (2020)

[160] Bao, H., Yu, X., Xu, Q., *et al.*: Three-dimensional memristive Morris–Lecar model with magnetic induction effects and its FPGA implementation. Cognitive Neurodynamics **17**, 1079–1092 (2023)

[161] Xu, Q., Wang, K., Feng, C., *et al.*: Dynamical effects of low-frequency and high-frequency current stimuli in a memristive Morris–Lecar neuron model. Chaos, Solitons and Fractals **189**, 115646 (2024)

[162] Yu, Y., Shi, M., Kang, H., *et al.*: Hidden dynamics in a fractional-order memristive Hindmarsh–Rose model. Nonlinear Dynamics **100**(1), 891–906 (2020)

[163] Xu, L., Qi, G., Ma, J.: Modeling of memristor-based Hindmarsh-Rose neuron and its dynamical analyses using energy method. Applied Mathematical Modelling **101**, 503–516 (2022)

[164] Zhang, J., Li, Z.: Switchable memristor-based Hindmarsh-Rose neuron under electromagnetic radiation. Nonlinear Dynamics **112**(8), 6647–6662 (2024)

[165] Li, K., Bao, H., Li, H., *et al.*: Memristive Rulkov neuron model with magnetic induction effects. IEEE Transactions on Industrial Informatics **18**(3), 1726–1736 (2022)

[166] Li, K., Bao, H., Li, H., *et al.*: Memristive rulkov neuron model with magnetic induction effects. IEEE Transactions on Industrial Informatics **18**(3), 1726–1736 (2022)

[167] Li, Y., Li, C., Lei, T., *et al.*: Offset boosting-entangled complex dynamics in the memristive Rulkov neuron. IEEE Transactions on Industrial Electronics **71**(8), 9569–9579 (2024)

[168] Xu, Q., Ju, Z., Ding, S., *et al.*: Electromagnetic induction effects on electrical activity within a memristive Wilson neuron model. Cognitive Neurodynamics **16**, 1221–1231 (2022)

[169] Njitacke, Z.T., Takembo, C.N., Koumetio, B.N., Awrejcewicz, J.: Complex dynamics and autapse-modulated information patterns in memristive Wilson neurons. Nonlinear Dynamics **110**(3), 2793–2804 (2022)

[170] Xu, Q., Wang, K., Shan, Y., *et al.*: Dynamical effects of memristive electromagnetic induction on a 2D Wilson neuron model. Cognitive Neurodynamics **18**(2), 645–657 (2024)

[171] Dong, Y., Wang, G., Chen, G., *et al.*: A bistable nonvolatile locally-active memristor and its complex dynamics. Communications in Nonlinear Science and Numerical Simulation **66**, 105203 (2020)

[172] Zhang, S., Li, C., Zheng, J., *et al.*: Memristive autapse-coupled neuron model with external electromagnetic radiation effects. IEEE Transactions on Industrial Electronics **70**(11), 11618–11627 (2023)

[173] Ying, J., Min, F., Wang, G.: Neuromorphic behaviors of VO_2 memristor-based neurons. Chaos, Solitons and Fractals **175**, 114058 (2023)

[174] Ma, J., Tang, J.: A review for dynamics in neuron and neuronal network. Nonlinear Dynamics **89**(3), 1569–1578 (2017)

[175] Wu, K., Huang, Z., Yan, M.: Dynamic behavior of memristor ML neurons and its application in secure communication. The European Physical Journal B **97**(7), 1–21 (2024)

[176] Zhang, S., Li, C., Zheng, J., *et al.*: Hidden coexisting hyperchaos of new memristive neuron model and its application in image encryption. IEEE Transactions on Industrial Electronics **158**, 112017 (2022)

[177] Rosenblatt, F.: The perceptron: a probabilistic model for information storage and organization in the brain. Psychological Review **65**(6), 386–408 (1958)

[178] Rumelhart, D.E., Hinton, G.E., Williams, R.J.: Learning internal representations by error propagation. Readings in Cognitive Science **323**(6088), 399–421 (1988)

[179] Hinton, G.E., Osindero, S., Teh, Y.W.: A fast learning algorithm for deep belief nets. Neural Computation **18**(7), 1527–1554 (2006)

[180] Yao, P., Wu, H., Gao, B., *et al.*: Fully hardware-implemented memristor convolutional neural network. Nature Publishing Group **577**, 641–646 (2020)

[181] Jeon, K., Ryu, J.J., Im, S., *et al.*: Purely self-rectifying memristor-based passive crossbar array for artificial neural network accelerators. Nature Communications **15**(1), 129 (2024)

[182] Maass, W.: Networks of spiking neurons: the third generation of neural network models. Neural Networks **10**(9), 1659–1671 (1997)

[183] Lu, S., Sengupta, A.: Exploring the connection between binary and spiking neural networks. Frontiers in Neuroscience **14**, 535 (2020)

[184] Pham, Q.T., Nguyen, T.Q., Hoang, B.C., et al.: A review of SNN implementation on FPGA. 2021 International Conference on Multimedia Analysis and Pattern Recognition (MAPR), Hanoi, Vietnam, 2021 (2021)

[185] Fida, A.A., Khanday, F.A., Mittal, S.: An active memristor based rate-coded spiking neural network. Neurocomputing **533**, 61–71 (2023)

[186] Bohte, S.M.: The evidence for neural information processing with precise spike-times: A survey. Natural Computing **3**(2), 195–206 (2004)

[187] Lisman, J., Buzsáki, G.: A neural coding scheme formed by the combined function of gamma and theta oscillations. Schizophrenia Bulletin **34**(5), 974–980 (2008)

[188] EL Bienenstock, L.C., Munro, P.: Theory for the development of neuron selectivity: orientation specificity and binocular interaction in visual cortex. Journal of Neuroscience **2**(1), 32–48 (1982)

[189] Diehl, P.U., Cook, M.: Unsupervised learning of digit recognition using spike-timing-dependent plasticity. Frontiers in Computational Neuroscience **99**, 99 (2015)

[190] Tavanaei, A., Masquelier, T., Maida, A.S.: Acquisition of visual features through probabilistic spike-timing-dependent plasticity. 2016 International Joint Conference on Neural Networks (IJCNN), Vancouver, BC, Canada, 2016 (2016)

[191] Faghihi, F., Cai, S., Moustafa, A.A.: A neuroscience-inspired spiking neural network for EEG-based auditory spatial attention detection. Neural Networks **152**, 555–565 (2022)

[192] Huang, P., Li, Z., Dong, Z., *et al.*: Binary resistive-switching-device-based electronic synapse with spike-rate-dependent plasticity for online learning. ACS Applied Electronic Materials **1**(6), 845–853 (2019)

[193] Neftci, E.O., Mostafa, H., Zenke, F.: Surrogate gradient learning in spiking neural networks: bringing the power of gradient-based optimization to spiking neural networks. IEEE Signal Processing Magazine **36**, 51–63 (2019)

[194] Wu, Y., Deng, L., Li, G., *et al.*: Spatio-temporal backpropagation for training high-performance spiking neural networks. Frontiers in Neuroscience **12**(12), 331 (2018)

[195] Taherkhani, A., Belatreche, A., Li, Y., Maguire, L.P.: DL-ReSuMe: a delay learning-based remote supervised method for spiking neurons. IEEE Transactions on Neural Networks and Learning Systems **26**(12), 3137–3149 (2015)

[196] Tavanaei, A., Maida, A.: BP-STDP: approximating backpropagation using spike timing dependent plasticity. Neurocomputing **330**, 39–47 (2019)

[197] Mozafari, M., Kheradpisheh, S.R., Masquelier, T., *et al.*: First-spike-based visual categorization using reward-modulated STDP. IEEE Transactions on Neural Networks and Learning Systems **29**(12), 6178–6190 (2018)

[198] Tang, G., Kumar, N., Yoo, R., Michmizos, K.P.: Deep reinforcement learning with population-coded spiking neural network for continuous control. Neurocomputing **330**, 39–47 (2019)

[199] Severa, W., Vineyard, C.M., Dellana, R., *et al.*: Training deep neural networks for binary communication with the Whetstone method. Nature Machine Intelligence **1**(2), 86–94 (2019)

[200] Huang, J., Serb, A., Stathopoulos, S., *et al.*: Text classification in memristor-based spiking neural networks. Neuromorphic Computing and Engineering **3**, 014003 (2023)

[201] Walters, B., Lammie, C., Yang, S., *et al.*: Unsupervised character recognition with graphene memristive synapses. Neural computing and applications **36**(4), 1569–1584 (2024)

[202] Yoon, R., Oh, S., Cho, S., Min, K.-S.: Memristor-CMOS hybrid circuits implementing event-driven neural networks for dynamic vision sensor camera. Micromachines **15**(4), 426 (2024)

[203] Wang, B., Zhang, X., Wang, S., *et al.*: Topology optimization of random memristors for input-aware dynamic SNN. Science Advances **11**(16), 5340 (2025)

[204] Hopfield, J., J.: Neural networks and physical systems with emergent collective computational abilities. Proc. Natl. Acad. Sci. U.S.A. **79**(8), 2554–2558 (1982)

[205] Hu, S.G., Liu, Y., Liu, Z., *et al.*: Associative memory realized by a reconfigurable memristive Hopfield neural network. Nature Communications **6**(6), 7522 (2016)

[206] Yu, F., Shen, H., Yu, Q., *et al.*: Privacy protection of medical data based on multi-scroll memristive Hopfield neural network. IEEE Transactions on Network Science and Engineering **10**(2), 845–858 (2023)

[207] G. Joya, M.A.A., Sandoval, F.: Hopfield neural networks for optimization: study of the different dynamics. Neurocomputing **43**(1), 219–237 (2002)

[208] Sami Doubla, I., Ramakrishnan, B., Tabekoueng Njitacke, Z., *et al.*: Hidden extreme multistability and its control with selection of a desired attractor in a non-autonomous Hopfield neuron. AEU: International Journal of Electronics and Communications **144**, 154059 (2022)

[209] Wang, M., Deng, B.: A multistable memristor and its application in fractional-order Hopfield neural network. Brazilian Journal of Physics **52**(6), 205 (2022)

[210] Bao, H., Hua, M., Ma, J., *et al.*: Offset-control plane coexisting behaviors in two-memristor-based Hopfield neural network. IEEE Transactions on Industrial Electronics **70**(10), 10526–10535 (2023)

[211] Li, C., Yang, Y., Yang, X., *et al.*: A tristable locally active memristor and its application in Hopfield neural network. Nonlinear Dynamics **108**(2), 1697–1717 (2022)

[212] Yu, F., Wu, C., Lin, Y., *et al.*: Dynamic analysis and hardware implementation of

multi-scroll Hopfield neural networks with three different memristor synapses. Nonlinear Dynamics **112**(14), 12393–12409 (2024)

[213] Chen, C., Bao, H., Zhang, Y., et al.: Synchronization and coupling dynamics in memristive homogeneous and heterogeneous Hopfield neural networks. IEEE Transactions on Circuits and Systems I: Regular Papers, 1–14 (2025)

[214] Lin, H., Wang, C., Tan, Y.: Hidden extreme multistability with hyperchaos and transient chaos in a Hopfield neural network affected by electromagnetic radiation. Nonlinear Dynamics **99**(3), 2369–2386 (2020)

[215] Fu, S., Wang, X., Gu, H., *et al.*: Multi-scroll Hopfield neural network under electromagnetic radiation and its brain-like coupling synchronization. Frontiers in Physics **11**, 1252568 (2023)

[216] Yao, W., Fang, J., Yu, F., *et al.*: Electromagnetic radiation control for nonlinear dynamics of Hopfield neural networks. Chaos **34**(7), 073149 (2024)

[217] Fu, S., Wang, X., Gu, H., *et al.*: Non-ideal memristor synapse-coupled bi-neuron Hopfield neural network: numerical simulations and breadboard experiments. AEU: International Journal of Electronics and Communications **111**, 152894 (2019)

[218] Chen, C., Min, F., Zhang, Y., Bao, B.: Memristive electromagnetic induction effects on Hopfield neural network. Nonlinear Dynamics **106**(3), 2559–2576 (2021)

[219] Ding, S., Wang, N., Bao, H., *et al.*: Memristor synapse-coupled piecewise-linear simplified Hopfield neural network: Dynamics analysis and circuit implementation. Chaos, Solitons and Fractals **166**, 112899 (2023)

[220] Yuan, R., Tiw, P.J., Cai, L., *et al.*: A neuromorphic physiological signal processing system based on VO_2 memristor for next-generation human-machine interface. Nature Communications **15**(4), 426 (2024)

[221] Bak, S., Park, J., Lee, J., Jeong, J.: Memristor-based CNNs for detecting stress using brain imaging signals. IEEE Transactions on Emerging Topics in Computational Intelligence **8**(1), 140–149 (2024)

[222] Li, Z., Yao, J., Zhang, B., et al.: VO_2 memristor-based adaptive neurons for electromyography signal processing. 2025 9th IEEE Electron Devices Technology and Manufacturing Conference (EDTM) Hong Kong, Hong Kong, 2025 (2025)

[223] Wu, X., Dang, B., Wang, H., *et al.*: Spike-enabled audio learning in multilevel synaptic memristor array-based spiking neural network. Advanced Intelligent Systems **4**(3), 2100151 (2022)

[224] Zhang, G., Fan, X., Wang, J., *et al.*: Self-rectifying memristors with high rectification ratio for attack-resilient autonomous driving systems. Nature Communications **16**(1), 5759 (2025)

[225] Biomedical Circuits, I.T., Systems: A memristive spiking neural network circuit for bio-inspired navigation based on spatial cognitive mechanisms. IEEE Transactions on Emerging Topics in Computational Intelligence **19**(3), 686–698 (2025)